Nucleotide-dependent displacement and dynamics of the α-1 helix in kinesin revealed by site-directed spin labeling EPR

(部位特異的スピンラベルEPR によるキネシンα-1 ヘリックスの

ヌクレオチド依存的変位と動的構造)

Doctoral thesis

January 2014

Satoshi Yasuda

安田哲

Department of Biological Science

Graduate School of Science

Osaka University

Preface

I would like to thank Elsevier publisher who allowed me to reuse my own article published by Elsevier following to Elsevier's copyright policy. My article has been published in:

Yasuda S., Yanagi T., Yamada M.D., Ueki S., Maruta S., Inoue A., Arata T. Nucleotide-dependent displacement and dynamics of α-1 helix in kinesin as revealed by site directed spin labeling EPR. Biochemical and Biophysical Research Communications Volume 443, Issue 3, 17 January 2014, Pages 911–916.

URL: http://www.sciencedirect.com/science/article/pii/S0006291X13021323

Contents

Abbreviations

$\boldsymbol{A}$, hyperfine interaction
Å, angstrom
AMPPNP, adenosine 5'-(β,γ-imido) triphosphate
$\boldsymbol{\beta}$, Bohr magneton
BCA, bicinchoninic acid
CW, continuous wave
DTT, dithiothreitol
DEER, the pulse double electron-electron resonance
$\Delta\boldsymbol{B}$, difference between interacting and non-interacting resonant peak
E. coli, *Escherichia coli*
EDTA, ethylenediaminetetraacetic acid
EGTA, ethylene glycol bis(2-aminoethyl ether)-tetraacetic acid
ESR, electron spin resonance
EPR, electron paramagnetic resonance
$\boldsymbol{g}$, g value or spectroscopic splitting factor
$\boldsymbol{h}$, Plank's constant
ME, mercaptoethanol
MT, microtubule
MSL, 4-maleimido-2,2,6,6-tetramethyl-1-piperidinoxy
MTSL, (1-oxyl-2,2,5,5-tetramethylpyrrolidin-3-yl) methanethiosulfonate
PAGE, poly acrylamide gel electrophoresis
PIPES, piperazine-1,4-bis(2-ethanesulfonic acid)
SDS, sodium dodecyl sulfate
SDSL, site directed spin labeling
$\boldsymbol{\tau_r}$, rotational correlation time
$\boldsymbol{\omega}$, Larmor frequency

Abstract

Kinesin is chemo-mechanical energy-transducing protein. For understanding of such energy transduction mechanisms, it is important to examine intra- and inter-molecular structures of these proteins during coordination between input and output. By using electron spin resonance (ESR) and spin labeling, I studied the ATP-induced conformational change of kinesin in intra-molecular structure.

I have used site-directed spin-labeling and ESR spectroscopy to monitor a nucleotide dependent conformational change of monomeric kinesin. Nitroxide spin label was placed in cys-lite kinesin5A (K349 monomer) at amino acid residue 62, 66, 67, 70, 72 or 114. These residues exist in α-1 helix and α-2 helix. The N-terminal residues of α-1 helix form a part of a nucleotide-binding pocket. And the C-terminal region of the helix is near the neck-linker. From the mobility of spin label, I detect more than two conformation of the α-1 helix.

Next, kinesin was doubly spin-labeled at the α-1 and α-2 helices, and the resulting EPR spectrum showed dipolar broadening. The inter-helix distance distribution showed that 20% of the spins have a peak

characteristic of 1.4-1.7 nm separation, which is similar to what is predicted from the x-ray crystal structure, albeit 80% were beyond the sensitivity limit (>2.5 nm) of the method. Upon microtubule binding, the fraction of kinesin exhibiting an inter-helix distance of 1.4-1.7 nm in the presence of AMPPNP (a non-hydrolysable ATP analog) and ADP was 20% and 25%, respectively. In the absence of nucleotide, this fraction increased to 40-50%. These nucleotide-induced changes in the fraction of kinesin undergoing displacement of the α-1 helix were found to be related to the fraction in which the neck-linker undocked from the motor core. It is therefore suggested that a shift in the α-1 helix conformational equilibrium occurs upon nucleotide binding and release, and this shift controls neck-linker docking onto the motor core.

I. General introduction

I.1 Protein conformation and function

Proteins exist in all cells and perform many functions within living organisms. The function of a protein often depends on the protein conformation. Therefore, many researchers have studied the conformations of proteins at atomic distance by using X-ray crystallography, nuclear magnetic resonance (NMR), electron microscopy (EM) and electron paramagnetic resonance (EPR).

Especially, site-directed spin labeling (SDSL)-EPR is a useful technique for investigating dynamics and conformation of protein and the protein complex with high molecular weight in solution. I studied the conformational change of kinesin on microtubules by using this SDSL-ESR method.

I.2 SDSL-EPR

Electron paramagnetic resonance spectroscopy (EPR), also called electron spin resonance (ESR), is a technique that detects unpaired spin. In 1989, group of Hubbell developed a new EPR strategy called site-directed spin labeling (SDSL)-EPR [Altenbach et al., 1989]. SDSL is a useful

technique for investigating dynamics and conformation of protein and protein complex. In SDSL-EPR method, a target amino acid residue is mutated to cysteine and covalently labeled with a specific reagent, nitroxide derivative (spin label) (Figure I-1) [Hubbell et al., 1998]. The EPR measurements of spin label provide several parameters such as the mobility of spin labeled side chains and distance between spin labels (Figure I-2) [Altenbach et al., 1989; Hubbell et al., 1998; Hubbell et al., 2000; Mchaourab et al., 1996; Rabenstein and Shin, 1995].

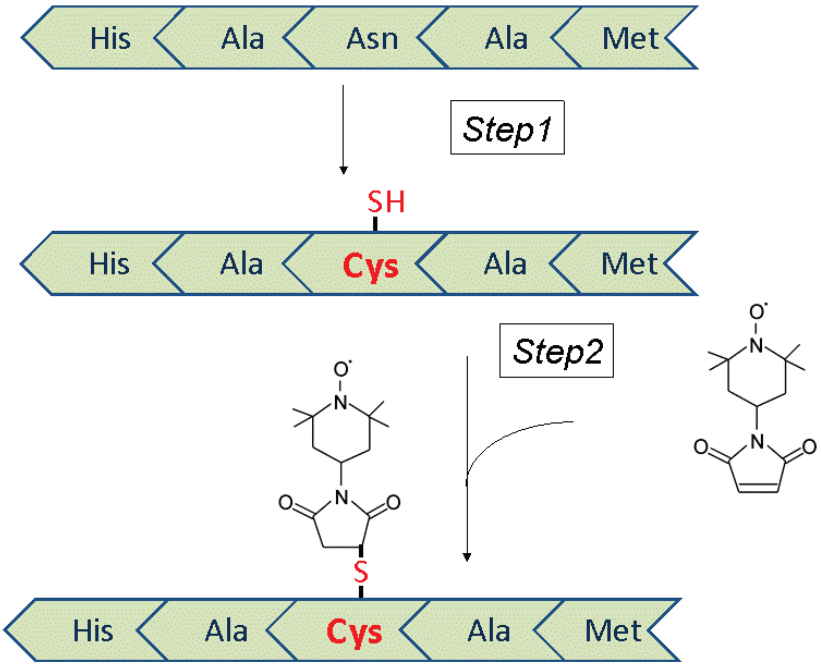

Figure I-1 In SDSL-EPR, a target residue is mutated to cysteine (*Step 1*) and spin-labeled with a specific reagent (*Step 2*). [Hubbell et al., 1998]

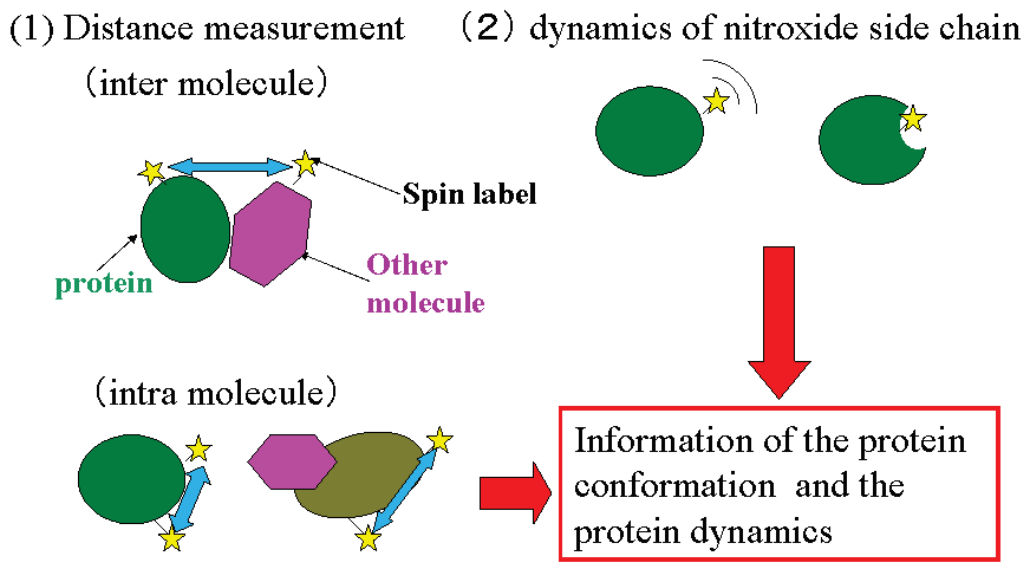

Figure I-2 Site-directed spin labeling (SDSL) is a useful tool for monitoring the dynamics and structure of the protein. [Altenbach et al., 1989; Hubbell et al., 1998; Hubbell et al., 2000; Mchaourab et al., 1996; Rabenstein and Shin, 1995]

I.2.1 Mobility

The line shape of the EPR spectrum depends on the rotational mobility of spin label on nanosecond time scale (Figure I-3) [Goldman et al., 1972]. The mobility of spin label depends on the steric hindrance around nitroxide side chain. Therefore, from the EPR spectra, the interaction sites between two proteins or the helix-helix contact within a protein molecule can be predicted (Figure I-3) [Mchaourab et al., 1996].

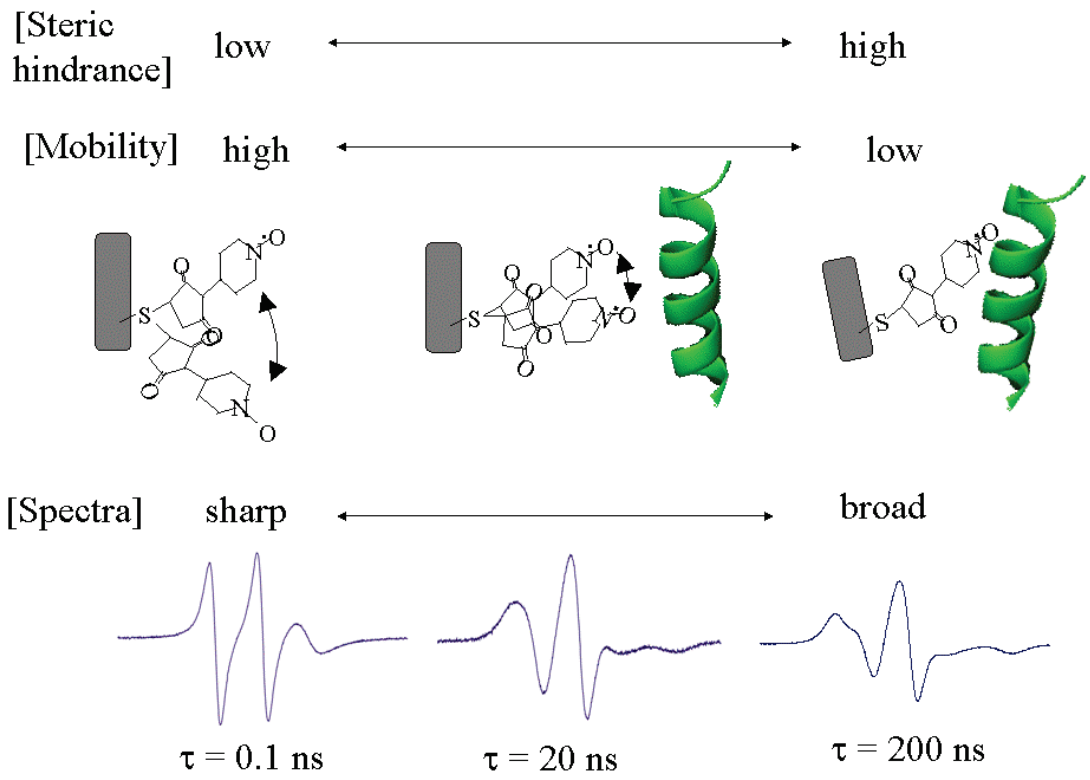

Figure I-3 The line shape of the EPR spectrum depends on the mobility of spin label. Rotational correlation times are about 0.1, 20 and 200 ns from sharp to broad spectrum. The EPR spectrum of nitroxide side chain is broadened when the spin label contacts with another molecule or domain or is buried inside the protein. [Goldman et al., 1972; Mchaourab et al., 1996]

I.2.2 Distance

The EPR spectrum of nitroxide side chain was broadened when another spin label is near the spin label (Figure I-4). Shin et al. developed a Fourier deconvolution method for EPR distance measurement [Rabenstein and Shin, 1995]. This method has been shown to provide accurate distributions of the distances between spin labels in the range from 0.8-2.5 nm [Rabenstein and Shin, 1995]. Dr. Arata and Dr. Fajer developed a new fitting method that calculates distance between two spin labels [Yamada et al., 2007; Sugata et al., 2009; Fajer et al., 2007]. In this method, the double labeled spectra were fit with the spectra simulated by convolution of single labeled spectra with broadening function determined from interspin distance distribution (See Section II for details).

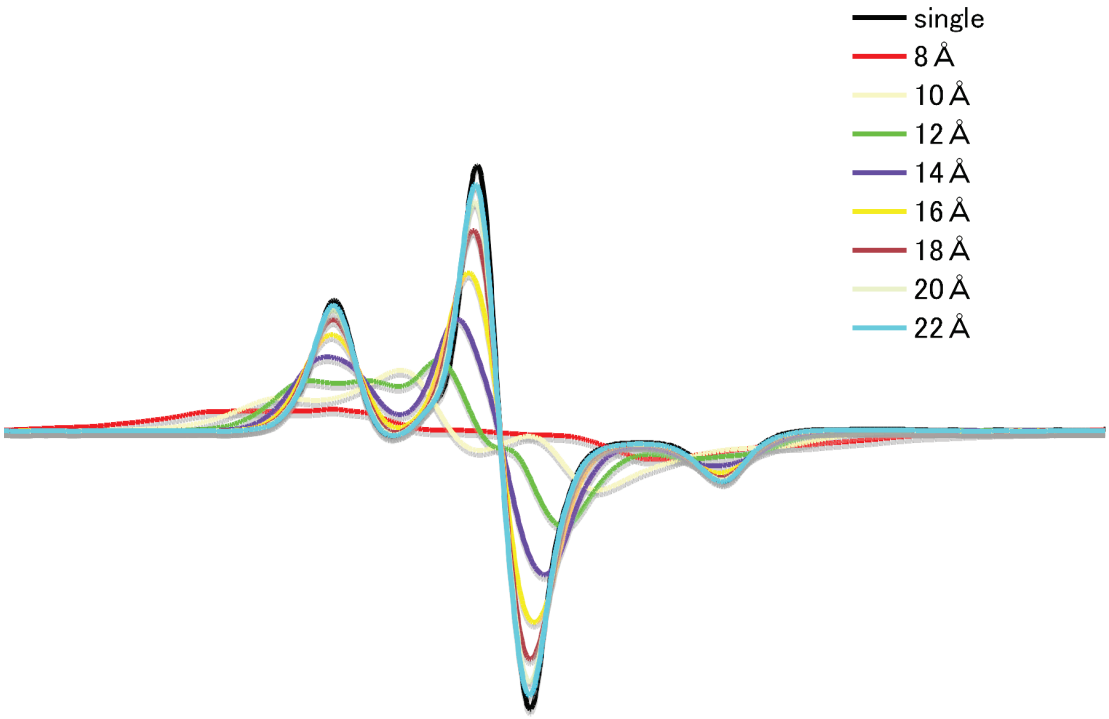

Figure I-4 Distance calculation between spin labels by CW-ESR spectral simulation. The EPR spectrum of nitroxide side chain is broadened when another spin label is near the spin label.

I.2.3 Comparisons with other methods

In comparison with X-ray crystallography, it is not necessary to make a crystal that is very difficult to make in some cases. SDSL-EPR detects the dynamic and distance information in solution without crystallization, but from local spin labeled residues.

In comparison with nuclear magnetic resonance (NMR), EPR needs incorporation of unpaired electron into protein with large molecular weight but detects a faster rotational mobility on nanosecond time scale which is similar to protein dynamics and side chain mobility, and much longer interspin distance (0.8-2.5 nm) which is similar to the distance between the tips of side chains at helices or domains within a protein or a protein complex.

In comparison with fluorescence measurement, both fluorescence depolarization and EPR detects the dynamics on nanosecond time scale. Fluorescence and EPR both detect polarity around environment of the labels. Polarity change sometimes causes large changes in fluorescence quantum yield but very small changes in hyperfine splitting of EPR spectrum. Fluorescence spectrum is complicated by substantial light scattering from

turbid proteins like microtubules.

As compared with fluorescence excitation resonance transfer (FRET), EPR has the following advantages. (1) No assumption concerning the orientation-dependent term have to be made (point dipole assumption is enough), whereas assumptions have to be made for the orientation factor κ in FRET measurements (usually $\kappa = 2/3$ for random orientation of fluorophores with high mobility). (2) The spin label used here is much smaller than fluorescence labels, leading to an easier correlation between measured distance and protein crystal structure. (3) The two spin labels can be identical, leading to easy double labeling on the same protein molecule or on the homodimer, whereas the donor and acceptor labels have to be different for FRET. In this study two identical spin labels were attached on the two mutated cysteines of kinesin monomer. (4) In FRET, other different mechanisms or light scattering from turbid proteins like microtubules lead to the fluorescence quenching and cause us to make spectral decomposition using additional measurement. On the other hand, in SDSL-EPR at low temperature (170K; in frozen state), no such spectral manipulations are made, although at room temperatures mobility difference for each spin labels

should be compensated by using a sum of each single-labeled spectra for single labeled spectrum.

I.3 Kinesin

The motor protein kinesin was discovered in 1985 by Vale et al. [Vale et al., 1985]. The motor protein kinesin moves processively along a microtubule (MT) while hydrolyzing ATP.

The kinesin superfamily is a large and diverse protein family, and its members are involved in a number of cellular processes such as cell division, movement of organelle and fast axonal transport [Vale et al., 1985; Brady, 1995; Hirokawa et al., 1998].

Conventional kinesin molecule consists of four polypeptide chains – two heavy chains and two light chains. Each heavy chain includes a C-terminal tail domain, a stalk domain and a motor domain (Figure I-5) [Verhey and Hammond, 2009]. The two motor domains of kinesin coordinate for processive motility. The hypothesis for the mechanism of processive movement is called the hand-over-hand model (Figure I-6) [Yildiz et al., 2004].

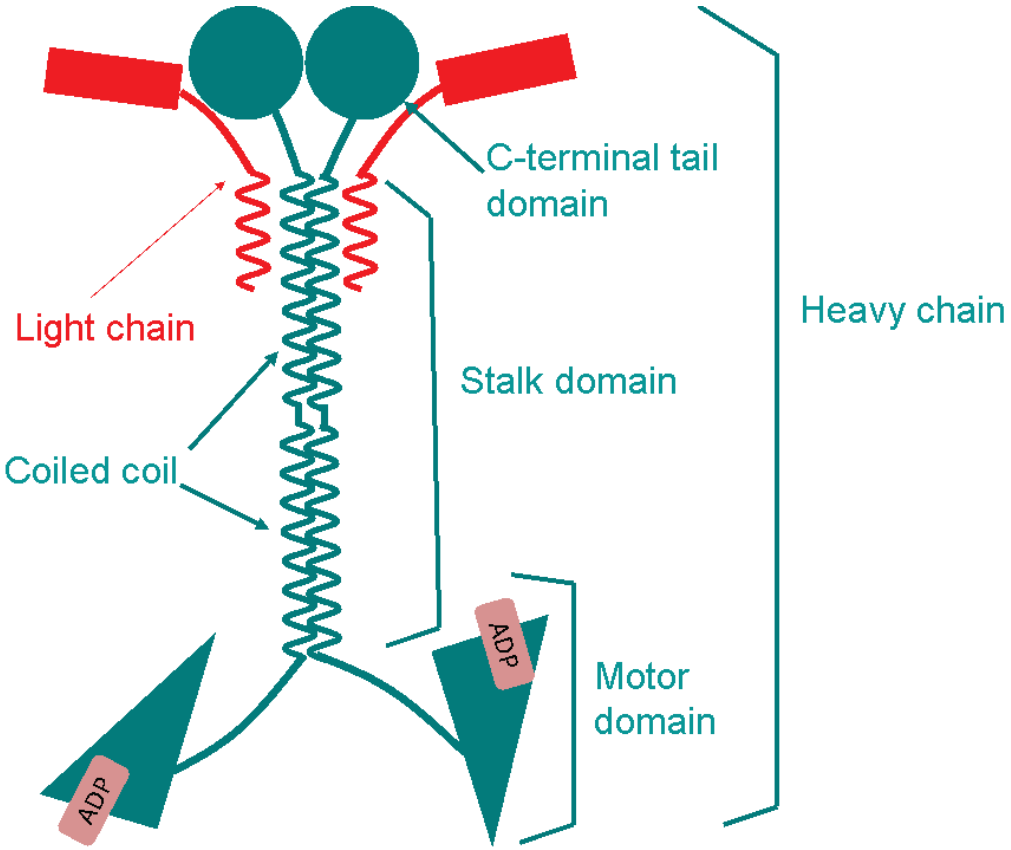

Figure I-5 Conventional kinesin damain model. Conventional kinesin molecule consists of four polypeptide chains – two heavy chains (green) and two light chains (red). Each heavy chain includes a C-terminal tail domain, a stalk domain and a globular head called the motor domain. Motor domains have nucleotide-binding pocket. In the figure, ADP binds to motor domain. [Verhey and Hammond, 2009]

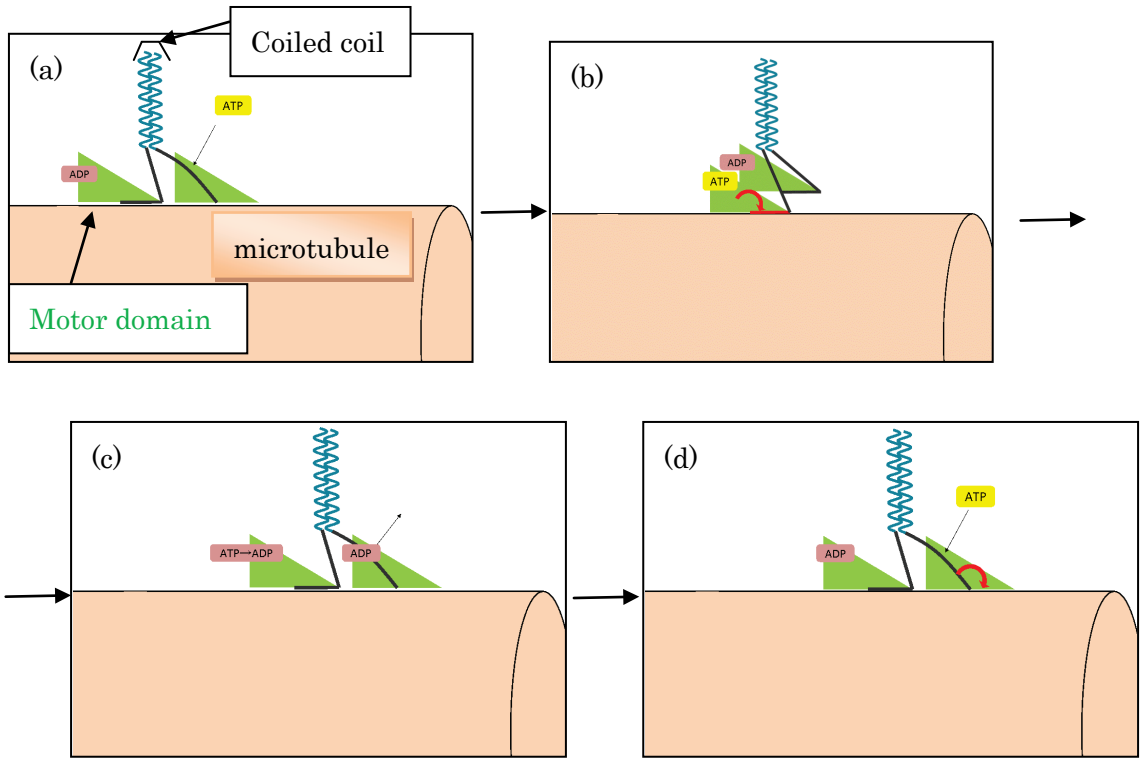

Figure I-6 Hand over hand model of kinesin movement. The green triangle models show the kinesin motor domains (motor heads). (a) ATP binds to the front head. (b) ATP binding leads to a conformational change of the front head. And the rear head unbinds from the microtubule and becomes a free head. (c) The free head binds to microtubule and become a new front head. And the new front head motor domain releases ADP. (d) ATP binds to the front head. [Yildiz et al., 2004; Rice et al.,1999]

Rice et al. proposed that neck linker plays an important role in the movement of kinesin [Rice et al.,1999]. The neck-linker is the link between the motor domain and the coiled-coil regions (Figure I-7). They showed that ATP binding facilitates the docking affinity of the neck linker to the catalytic motor core. This region has been shown to be important for force generation and directionality [Rice et al.,1999; Tomishige and Vale, 2000; Sindelar et al., 2002; Rice et al., 2003]. Crystal structures of the motor domains of kinesin-1 (conventional kinesin) and kinesin-related proteins show conformational changes that depend on the nucleotide binding to the motor domain [Kull et al., 1996; Nitta et al., 2004; Nitta et al., 2008].

Sugata et al. reported the interspin distances between two neck linkers in dimeric kinesin on microtubules [Sugata et al., 2009] as well as the mobility of neck linkers of monomeric kinesin on microtubules [Rice et al.,1999; Sindelar et al., 2002; Rice et al., 2003]. They found that the transition of the neck linker from an undocked to a docked conformation occurred in the ATP-bound state but not in the ADP-bound state or no nucleotide state, suggesting that the neck linker is an ATP- and strain-dependent mechanical element.

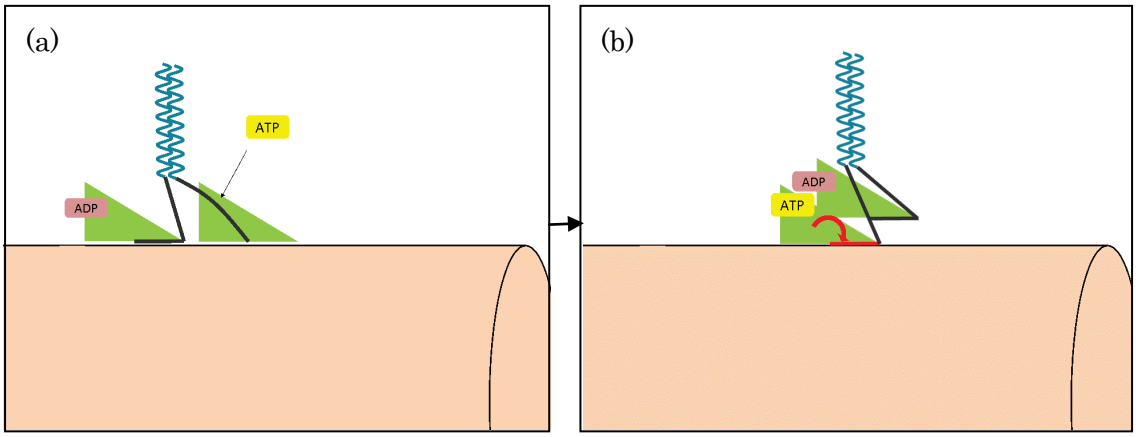

Figure I-7 The neck-linker plays an important role in the movement of kinesin. The neck-linker (red) links the motor domain (green triangle) to the coiled-coil dimerization domain (cyan). Orange column models show microtubules. (a) ATP binds to the front head. (b) The binding of ATP causes the neck-linker region to dock on the motor domain and then pull the rear head forward on a microtubule (orange column). [Rice et al.,1999]

I.4 Energy transducing mechanism

As mentioned in the Section I.3, the kinesin ATPase family hydrolyzes the ATP in coordination with kinesin conformational changes, which results in mechanical work of cell. Rice et al. proposed that neck linker plays an important role in the movement of kinesin [Rice et al.,1999]. However, it remains to be solved how kinesin convert ATP energy into work at submolecular or atomic level in the presence of microtubules. Therefore, it is important to understand how nucleotides (ATP or ADP) bound in the active catalytic site can communicate with the neck-linker to control neck-linker docking on the kinesin core domain. Recent cryoelectron microscopy (cryo-EM) studies also revealed that these unique two helices, switch I and switch II, communicate between the P-loop of catalytic site and the neck-linker docking region [Kikkawa et al., 2001; Hirose et al., 2006; Vale, 1996; Sindelar and Downing, 2007; Sindelar and Downing, 2010]. The SDSL-EPR studies also suggested that switch I and switch II undergo nucleotide-dependent conformational changes (analogous to conformational changes in G-proteins) that play an important role in communicating between the catalytic site (P-loop) and the neck-linker docking domain on the

MT-binding interface of kinesin [Naber et al., 2003].

In kinesin X-ray crystal structures, the N-terminal region of the α-1 helix is adjacent to the adenine ring of the bound adenine nucleotide, while the C-terminal region of the helix is near the neck-linker (Figure I-8) [Sack et al., 1997]. It is therefore hypothesized that the α-1 helix plays an important role in communicating between the adenine ring occupancy and the neck-linker docking domain by the way different from that through switch I and switch II associated with γ-phosphate occupancy at P-loop. Here, I examined, using SDSL-EPR, the displacement of the α-1 helix relative to the α-2 helix of a kinesin monomer bound to MTs in the presence or absence of nucleotides. EPR measurements allowed direct and quantitative measurement of the mole fraction of the helix structural states and thus of the equilibrium constants for the critical nucleotide-dependent helix movements. It is found that a shift in the equilibrium between two α-1 helix conformations occurs upon nucleotide binding and release at catalytic active site (adenine-ring binding site) and that this shift controls neck-linker docking onto the motor core.

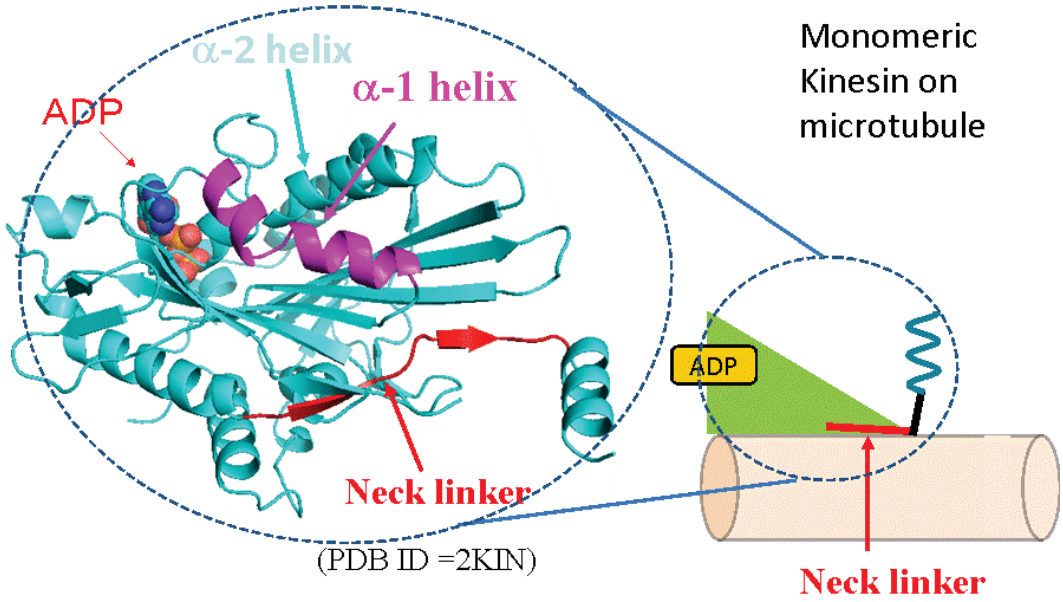

Figure I-8 The X-ray crystal structure of rat kinesin motor domains reported by Sack et al. (PDB ID : 2KIN) [Sack et al., 1997]. The N-terminal region of the α-1 helix (purple) is adjacent to the adenine ring of the bound adenine nucleotide (space-filling model indicated by ADP), while the C-terminal region of the helix is near the neck-linker (red).

II　Materials and Methods

II.1 Kinesin mutagenesis, purification, labeling, and ATPase activity measurements

I prepared the wild-type kinesin construct (Cys-lite) and site-directed mutants as described previously (Figure II-1) [Yamada et al., 2007]. Wild-type and mutant kinesins were expressed in *Escherichia coli* and purified using cobalt affinity chromatography as described previously [Sugata et al., 2004]. Kinesin (at approximately 20 to 50 μM) was incubated with 3-fold excess MSL, 4-maleimido-2,2,6,6-tetramethyl-1-piperidinyloxy (Sigma), for 8 hours at 4°C in a solution containing 25 mM PIPES-NaOH (pH 7.0), 50 mM NaCl, 2 mM $MgCl_2$, 100 μM ADP, and 3% N,N-dimethylformamide (Figure I-1). The free spin-label was removed by filtration on a Sephadex G25 column using a buffer containing 25 mM PIPES-NaOH (pH 7.0), 50 mM NaCl, 2 mM $MgCl_2$, 100 μM ADP, 1 mM ethylene glycol-bis(l-aminoethyl ether)-N,N,N′,N′-tetraacetic acid (EGTA), and 1 mM β-mercaptoethanol (ME). For formation of the kinesin–MT complex, 30 μM spin-labeled kinesin was mixed with 200 μM polymerized tubulin [Sugata et al., 2009], and the samples were centrifuged and resuspended in buffer containing the nucleotide of interest. For the EPR

measurements, the kinesin-MT complex was incubated with either 2 mM adenosine 5'-(β,γ-imido)triphosphate (AMPPNP), 2 mM ADP, or 5 U/ml apyrase. The concentration of the kinesin preparation for EPR measurements was approximately 50 μM.

To measure the MT-activated ATPase activity of each mutant kinesin, 0.1 μM kinesin was incubated with MTs (varying in concentration from 0 to 20 μM) and 1 mM ATP in 25 mM PIPES-NaOH (pH 7.0), 50 mM NaCl, 2 mM $MgCl_2$, 1 mM EGTA, and 1 mM βME at 25°C [Yamada et al., 2007; Ueki et al., 2005].

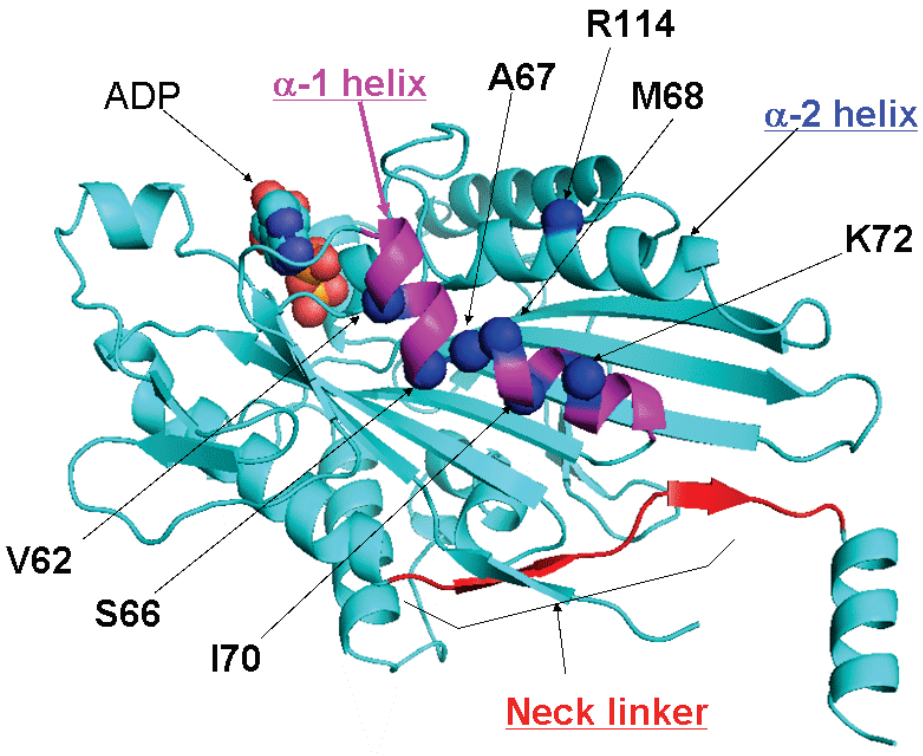

Figure II-1 Location of site-directed mutagenesis in the crystal structure of the kinesin motor domain (2KIN). The V62, S66, A67, M68, I70, K72 and R114 residues of mouse kinesin were mutated to cysteine and spin labeled. The mutated residues are represented by blue spheres. ADP is shown as a space-filling model.

II.2 EPR spectroscopy

II.2.1 The ratio of spin label to protein

CW(continuous wave)-EPR measurements were performed with a Bruker ELEXSYS E500 spectrometer (Bruker Biospin, Billerica, MA) as described previously [Yamada et al., 2007; Ueki et al., 2005]. The number of spins was estimated by the double integration of the EPR signal, while protein concentration was measured by the Bio-Rad Protein Assay (Bio-Rad Laboratories, Tokyo, Japan). The ratio of spin label to protein was determined from the two parameters.

II.2.2 Mobility

The effective rotational correlation time was calculated according to the equation of Goldman *et al.* [Goldman et al., 1972]: $\tau_r = a(1-T_{eff}/T_{max})^b$, where $a = 5.4 \times 10^{-10}$ s, $b = -1.36$, $T_{max} = 35$ G is the rigid limit for a particular spin, and $2T_{eff}$ is the effective splitting between the low-field and high-field absorption peaks (Figure II-2). Assuming that the experimental spectra contain only two single components corresponding to the fast and slow motion of the spin label, I estimated a ratio of peak height between the slow and fast components at a lower magnetic field as an indicator of steric

hindrance around the side chains (Figure II-3).

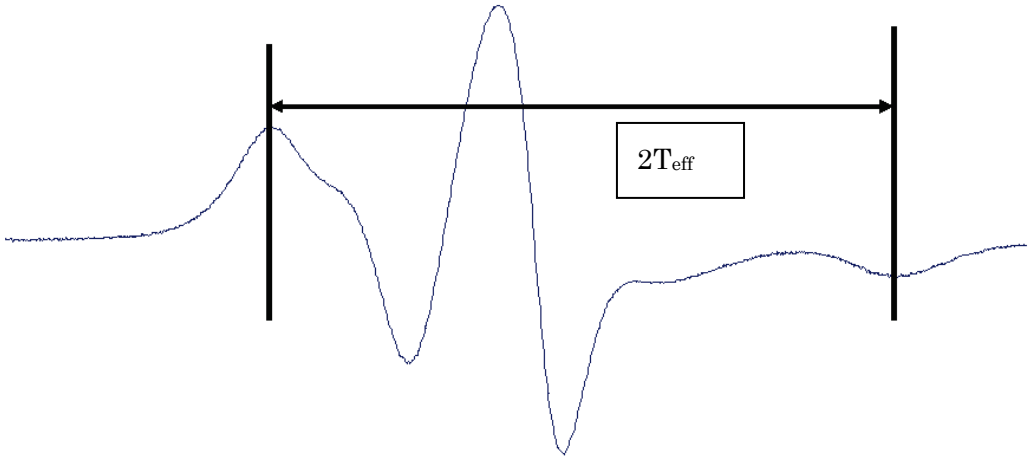

Figure II-2 Example of EPR spectrum with estimation of T_{eff}. [Goldman et al., 1972]

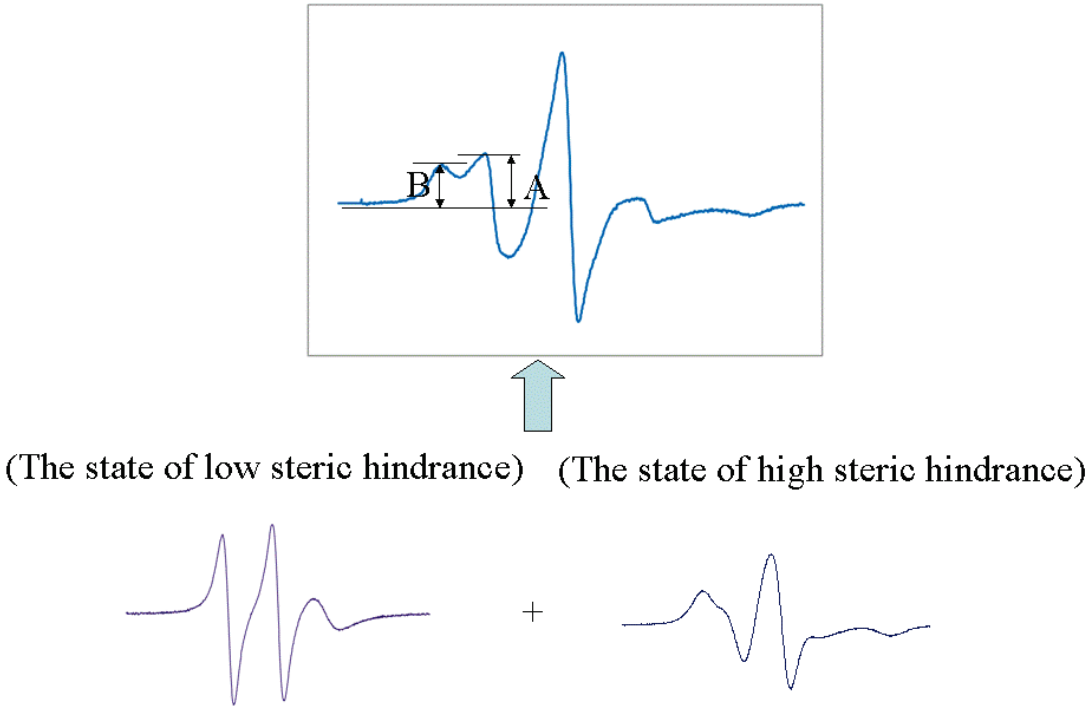

Figure II-3　A ratio of peak height between the slow and fast components at a lower magnetic field as an indicator of steric hindrance around the side chains.

II.2.3 Distance measurement

As described in Section I.2.2, the dipolar EPR method has been shown to provide accurate distributions of the distances between spin labels in the range from 0.8-2.5 nm [Rabenstein and Shin, 1995]. To eliminate broadening by the motional effect, the spectra were obtained in frozen solutions at 173 K. The dipolar spectrum is a convolution of the spectrum with no spin-spin interactions (single-labeled spectrum) with a broadening function ΔB: $\Delta B = \pm D/(R_{AB})^3$. R_{AB} is the electron-electron distance between two spin (A and B). D is the parameter calculated from g factors of respective electrons, Bohr magneton and the angle between the line connecting the loci of both electrons and the magnetic field $\mathbf{B}_0$ axis (Figure II-4). This angle is assumed to be random (isotropic orientation). The EPR data were fit successfully by changing 3 parameters: the center and full-width at half maximum of the distance distribution between the spin labels (modeled as single Gaussian) and the fraction of non-interacting spins [Yamada et al., 2007; Sugata et al., 2009; Fajer et al., 2007]. Fitting with two or three Gaussians was also performed. Goodness of fit was evaluated by the residual

sum (χ^2). Spectral broadening of the double-labeled samples was analyzed using a Levenberg-Marquardt algorithm in software written in Igor Pro (Wavematrix, Inc, Lake Oswego, OR) developed in our laboratory [Yamada et al., 2007] and confirmed using a Monte Carlo/Simplex Gaussian convolution method in software CWdipFit [Sugata et al., 2009; Fajer et al., 2007] (Figure II-5).

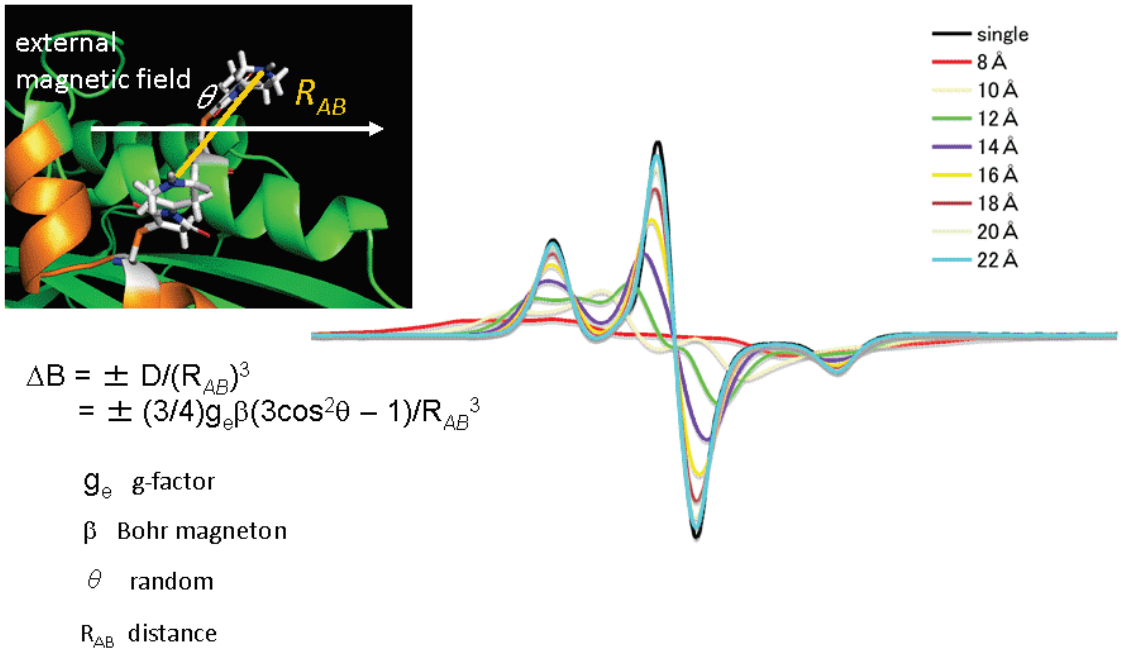

Figure II-4 Distance calculation between spin labels by CW-ESR spectral simulation. The EPR spectrum of nitroxide side chain is broadened when another spin label is near the spin label. Simulation temperature was 170K. [Rabenstein and Shin, 1995; Yamada et al., 2007; Sugata et al., 2009; Fajer et al., 2007; Ueda, 2012]

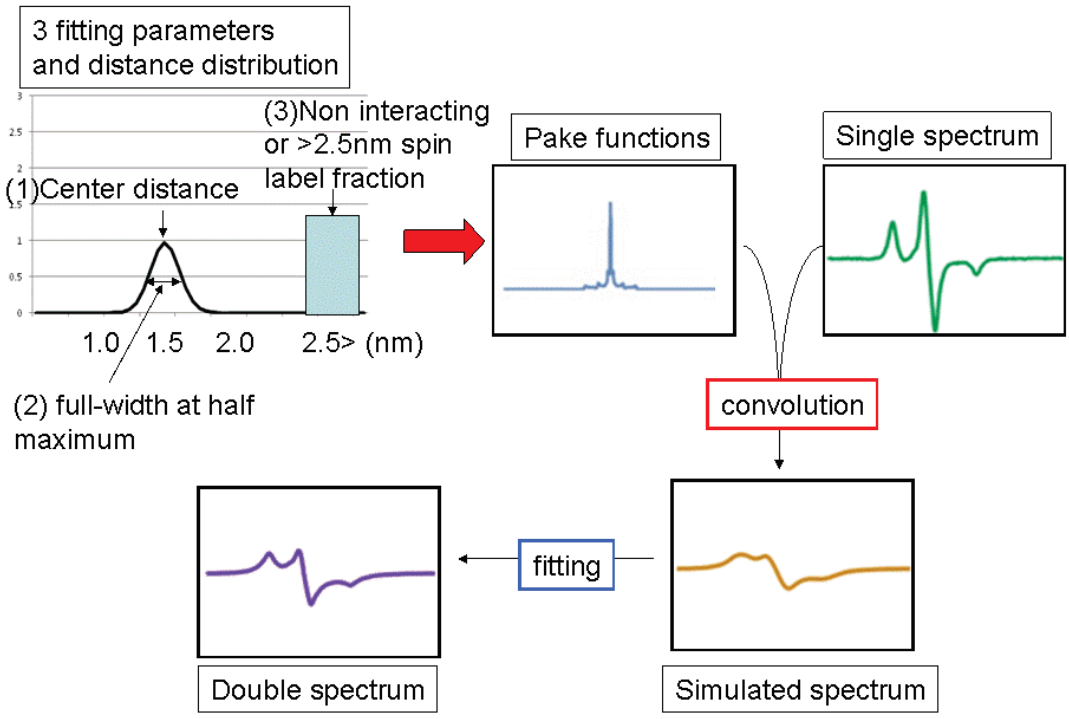

Figure II-5 The diagram showing the fitting method for distance calculation between two spin labels. [Yamada et al., 2007; Sugata et al., 2009; Fajer et al., 2007; Ueda, 2012]

III Results and Discussion

III.1 Functional properties of labeled kinesin mutants

I spin-labeled 7 kinesin mutants (V62C, S66C, A67C, M68C, I70C, K72C, R114C) with mutations in the α-1 and α-2 helices with MSL (Figures II-1 and I-1). The labeling efficiency for kinesin, estimated from double integration of the spectrum, was > 0.9 mol/mol cysteine residue.

I measured the MT-dependent ATPase activity of spin-labeled kinesin (Table III-1). The MT-dependent ATPase activities (V_{max}) of the spin-labeled mutants were more than 50% of that of the WT Cys-lite kinesin. Furthermore, the ATPase activity in the presence of MTs was at least 600 times higher than basal ATPase activity. These results suggested that all the kinesin mutants retained near wild-type MT-dependent ATPase activity.

Table III-1 Basal and MT-dependent V_{max} ATPase activity of spin-labeled kinesin mutants.

Sample	basal ATPase (s^{-1})	V_{max}(s^{-1}) [a]
Cys-lite[b]	0.013	27.5
V62C	0.022	13.9
S66C	0.030	17.9
A67C	0.027	16.5
M68C	0.010	19.3
I70C	0.011	18.9
K72C	0.010	25.1
R114C	0.020	24.6
K72C/R114C	0.012	18.0

[a] V_{max} was determined by measuring the ATPase rate in the presence of at least two saturating concentrations of MTs (10 and 20 μM).

[b] Not spin-labeled.

III.2 Nucleotide-dependent changes in the mobility of spin-labeled α-1 helix and α-2 helix side chains

I investigated the effect of bound MTs on the EPR spectra from kinesins mutated at the residues in the α-1 helix and α-2 helix in the ADP-bound state (Figure III-1). The spectrum of the kinesin mutant spin-labeled at V62C on the α-1 helix in the ADP-bound state in the absence of MTs showed a mixture of fast and slow components. The effective rotational correlation time of the fast and slow components were nearly 1.50 ns and 19.4 ns, respectively. The peak height ratio of the fast to slow components was 1.13. Assuming that the height of the slow mobility peak represents approximately twice as many labels as the same height for fast mobility peak, then the fraction of the fast component was estimated to be 36%. These results indicated that the side chain of the V62C residue of the kinesin α-1 helix could have two conformations. When the spin-labeled V62C mutant was mixed with MTs, the EPR spectrum again showed a mixture of fast and slow components. However, the peak height ratio decreased to 0.50, and as a result, the fraction of fast components decreased to 20%. Other kinesin mutants showed the same tendency (Table III-2). These results

indicated that binding of MTs to the kinesin motor domain caused a conformational change in the α-1 and α-2 helix regions, and these changes resulted in enhanced steric hindrance around these residues and/or reduced flexibility of the backbone of these helices.

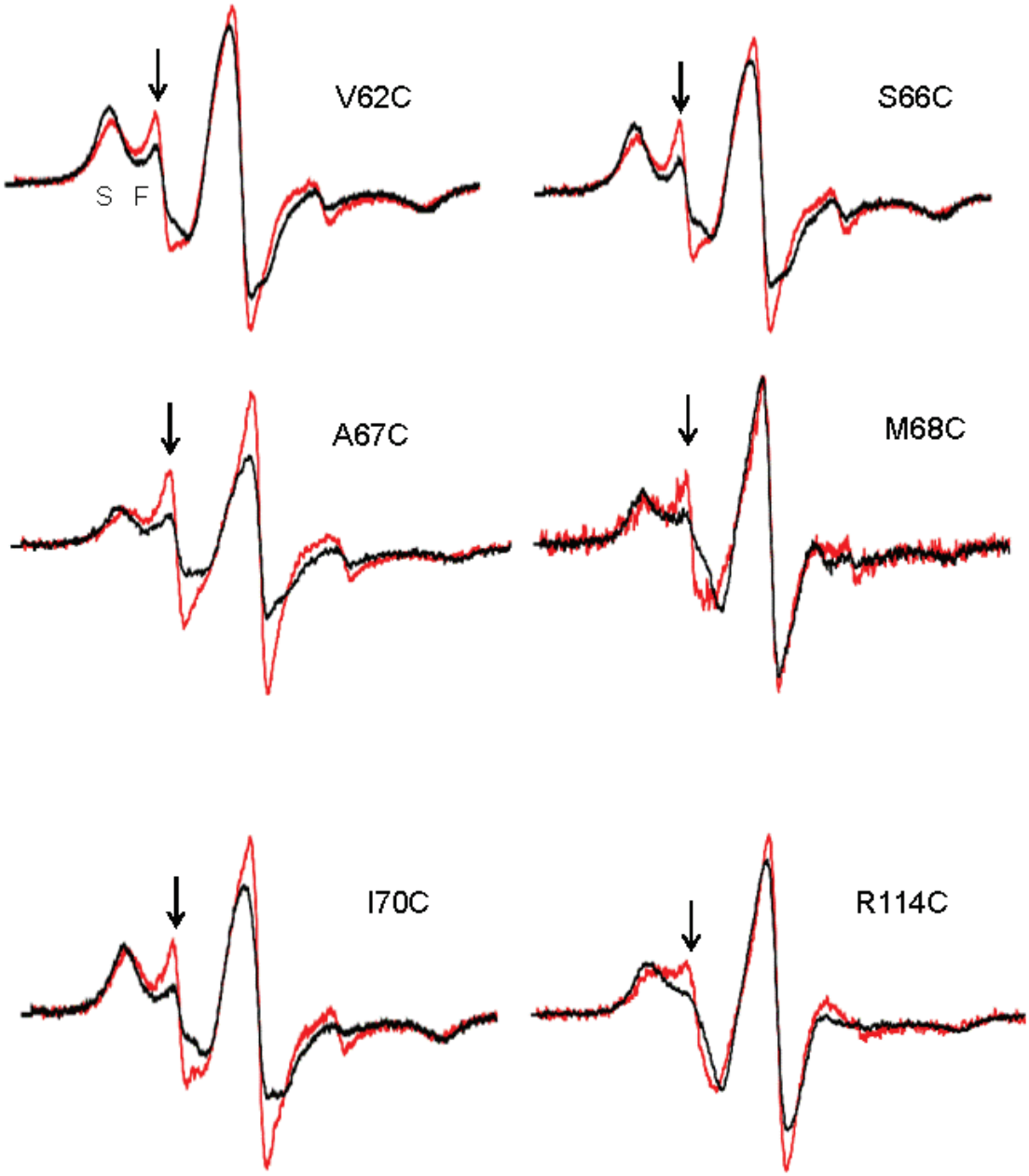

Figure III-1 Overlaid EPR spectra from spin labels attached to the V62C, S66C, A67C, M68C, I70C and R114C mutants in the presence or absence of MT. The spectra were taken at room temperature in the ADP-bound state both with (red line) or without (black line) MT. The scan width is 100G. The arrows show the peaks indicating significant spectral change.

Table III-2 Summary of the effective rotational correlation time (τ_r) of the spin-labeled kinesin residues

		τ_r (ns)			
mutant	component	ADP	ADP+MT	AMPPNP+MT	NN(+apyrase)+MT
V62C	Fast	1.50 (36%)[a]	1.52 (20%)	1.45 (22%)	1.46 (20%)
	Slow	19.4 (64%)	35.3 (80%)	28.1 (78%)	29.1 (80%)
S66C	Fast	1.48 (38%)	1.47 (20%)	1.46 (21%)	1.45(19%)
	Slow	16.6 (67%)	42.1 (80%)	38.5 (79%)	34.0 (81%)
A67C	Fast	1.43 (49%)	1.47 (29%)	1.46 (31%)	1.47 (31%)
	Slow	18.1 (51%)	19.1 (71%)	21.2 (69%)	31.4 (69%)
M68C	Fast	1.42 (44%)	1.46(24%)	1.46 (19%)	1.48 (15%)
	Slow	10.9 (56%)	12.3 (76%)	15.0 (81%)	16.4 (85%)
I70C	Fast	1.45 (36%)	1.46 (17%)	1.47 (17%)	1.48(15%)
	Slow	23.7 (64%)	40.6 (83%)	41.8 (83%)	36.8 (85%)
K72C	Fast	-	1.48 (39%)	1.51 (40%)	1.49 (36%)
	Slow	-	27.4 (61%)	23.3 (60%)	39.3 (64%)
R114C	Fast	1.46 (34%)	1.50 (17%)	1.52 (21%)	1.52 (14%)
	Slow	6.41 (66%)	8.89 (83%)	10.8 (79%)	7.44 (86%)

[a]Values in parentheses are the proportions of the fast and slow components.

I also examined the effect of nucleotide binding on spin label mobility in the α-1 helix side chains in the presence of MTs (Figures III-2 and III-3). In these experiments, the absorption line shapes of all mutants also had two components. The effective rotational correlation times of the fast and slow components, nearly 1.5 ns and 10-40 ns, respectively, were similar among all mutants in the presence of various nucleotides. The fraction of the fast component in the kinesin mutants labeled at V62C, S66C, A67C, M68C, I70C, K72C, and R114C with no nucleotide (NN) was 20%, 19%, 31%, 15%, 15%, 36%, and 14%, respectively (Table III-2). For these mutants in the ATP analogue(AMPPNP)-bound state, the fraction of the fast component was estimated to be 22%, 21%, 31%, 19%, 17%, 40%, and 21%, respectively. For these residues in the ADP-bound state, the fraction of the fast component was estimated to be 20%, 20%, 29%, 24%, 17%, 39%, and 17%, respectively. Therefore, the fraction of the fast component in the NN state obtained from the M68C, K72C, and R114C mutants was smaller than in the AMPPNP- or ADP-bound state. These results indicated that the binding of AMPPNP or ADP caused a conformational change of the α-1 and α-2 helix regions, eliminating steric hindrance around these residues.

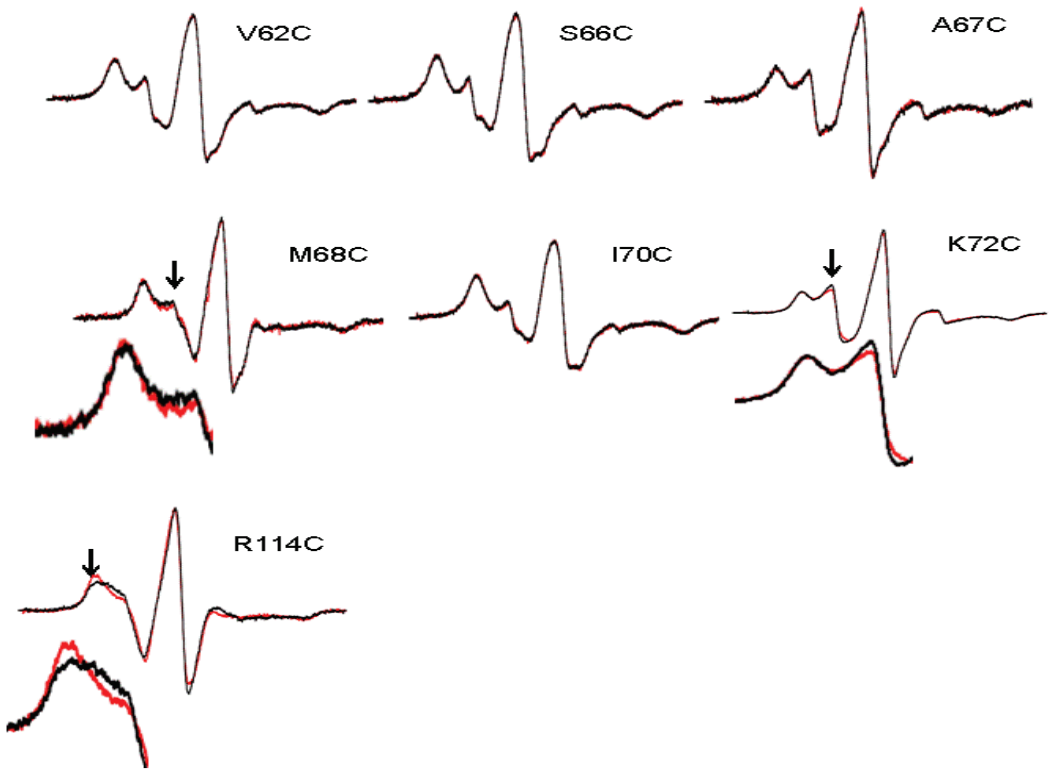

Figure III-2 Overlaid EPR spectra from spin labels attached to the V62C, S66C, A67C, M68C, I70C, K72C and R114C mutants in AMPPNP-bound or apo state. The spectra were taken at room temperature in the AMPPNP-bound state (black line) and the apo or no nucleotide (NN) state (red line) with MT (See Section II). The arrows show the peaks indicating significant spectral change. The insets show the magnified spectra at lower magnetic field, indicating significant change. All other conditions are as described in the legend of Figure III-1.

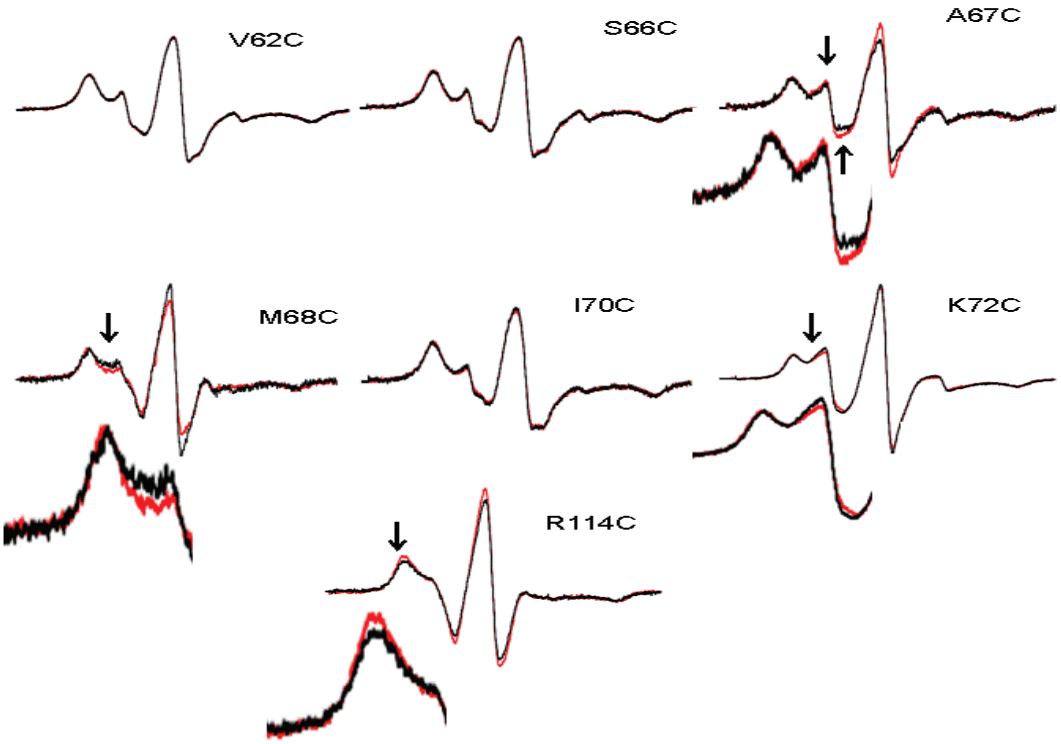

Figure III-3 Overlaid EPR spectra from spin labels attached to the V62C, S66C, A67C, M68C, I70C, K72C and R114C mutants in the ADP-bound or apo state. The spectra were taken at room temperature in the ADP-bound state (black line) and the apo or NN state (red line) with MT (See Section II). The arrows show the peaks indicating significant spectral change. The insets show the magnified spectra at lower magnetic field, indicating significant change. All other conditions are as described in the legend of Figure III-1.

III.3 Determination of interspin distances between M68C and R114C in the absence and presence of Microtubules (MTs)

I measured dipolar interactions between two spin labels located at residues M68C and R114C using dipolar EPR spectroscopy to detect the conformational change of the kinesin α-1 helix induced by nucleotide-binding in the presence or absence of MTs. Figure III-4 shows the spectra of double-labeled kinesin in the ADP-bound state in the absence of MTs at 173K. A comparison of the double-labeled EPR spectrum for the MT-free kinesin with the spectrum of the single-labeled kinesin revealed clear spectral line broadening. The amplitude of the double-labeled spectrum appeared smaller (86%) than that of the single-labeled spectrum. This observation indicated that the spin-spin distances were less than 2.5 nm. Distance distributions were obtained using a spectral fitting method by assuming a single Gaussian distribution of distances and non-interacting spins (>2.5 nm) (Figure III-4, left). The result showed a narrow Gaussian distribution centered at 1.40 nm with a full-width at half maximum of 0.07 nm (Figure III-4, right). However, 79% of spins were beyond the sensitivity

limit of the dipolar CW-EPR method (>2.5 nm), including a small amount of non-interacting spins (<10%) due to substoichiometric spin-labeling efficiency. The single Gaussian fits without assuming a population of >2.5 nm spins did not result in well-defined narrow distributions, as evidenced by the residual sum (χ^2) becoming 10-20% worse (data not shown). Fitting with two or three Gaussians did not result in a better fit (data not shown). These results demonstrated that the distribution of distances between the two spin labels attached at M68C and R114C has two different components. This result strongly suggested that the relative positions, at least the relative residual positions of the two helices, have two populations: one (21%) having a narrow inter-helix distance distribution centered at 1.4 nm and the remaining second population (79%) having an inter-helix distance beyond the 2.5-nm limit of detection. The narrow distance distribution (1.4 nm) is close to the 68Lys Nζ - 114His $N\varepsilon_2$ distance (1.49 nm), the 68Lys Cβ - 114His Cβ distance (1.14 nm), and the 68Lys Cα - 114His Cα distance (1.11 nm) from the crystal structure (2KIN) reported by Sack et al. [Sack et al., 1997]. However, the conformation with an inter-helix distance beyond sensitivity (>2.5 nm) is unexpected. Therefore, it is likely that either or both of the

kinesin α-1 and α-2 helices fluctuate between long and short inter-helix distance states.

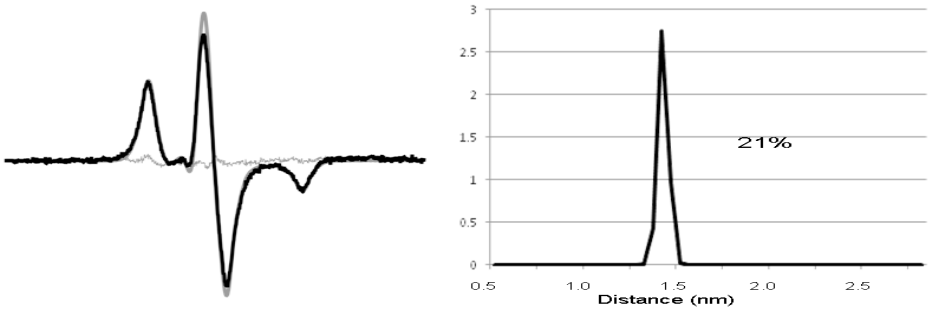

Figure III-4 Distance analysis of the EPR spectra from the double-labeled K68C/R114C kinesin mutant in the absence of MT. The EPR spectra of the ADP-bound state were obtained at 173K without MTs (See Material and Methods). The left panel compares the experimental spectrum of the double-labeled kinesin mutant (black line) with the spectrum of the single-labeled mutant (thick gray line) normalized to the same number of spins. The experimental spectra are fitted satisfactorily by a single Gaussian distance distribution (right panel) with some fraction of spins occurring beyond the sensitivity limit (>2.5 nm). The percentages shown are the fraction of the total spins with an inter-helix distance characterized by the single Gaussian distribution: 100 x (1 - fraction of spins >2.5 nm apart). Residuals from the best-fit spectra (thin gray lines) are shown on the left panel.

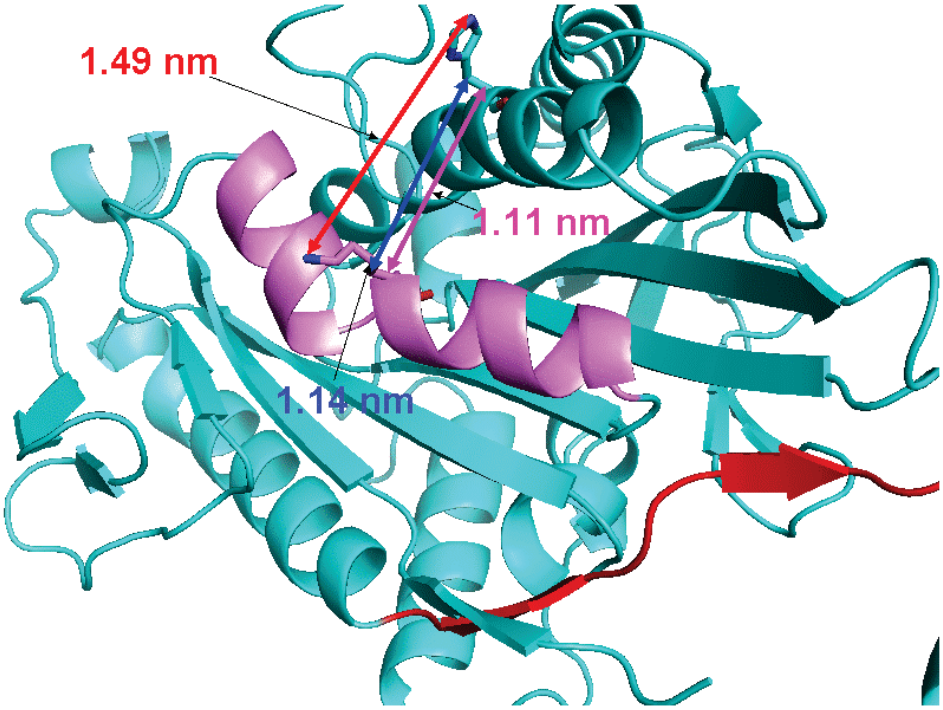

Figure III-5 Molecular distances and X-ray structure (2KIN). The narrow distance distribution (1.4 nm) of EPR spectrum analysis is close to the 68Lys Nζ - 114His $N\varepsilon_2$ distance (1.49 nm), the 68Lys Cβ - 114His Cβ distance (1.14 nm), and the 68Lys Cα - 114His Cα distance (1.11 nm) from the crystal structure (2KIN) reported by Sack et al. [Sack et al., 1997].

To investigate the different ATP hydrolysis intermediates of the double-labeled kinesin mutants in the presence of MTs, three nucleotide conditions were used: (i) an ADP-bound state, (ii) an AMPPNP-bound state, and (iii) an apo state in the absence of any nucleotide [no-nucleotide (NN)]. These data are shown in Figures III-6, III-7 and III-8, respectively. And Table III-3 shows summary of Figures III-4, III-6, III-7 and III-8. In all cases, the EPR spectra were again broadened, implying that the spin–spin distances were less than 2.5 nm. The spectrum obtained in the presence of AMPPNP is very similar to that obtained in the MT-free state. In fact, there was a population (20%) with its distribution centered at 1.43 nm with a full-width at half maximum of 0.13 nm; the remaining fraction of spins (80%) was beyond the sensitivity limit of the method (>2.5 nm). In the no-nucleotide (NN) state, the spectrum was different and much broader. There was a larger population (41%) having a somewhat narrow distribution (full-width at half maximum=0.41 nm) centered at 1.48 nm, and the remaining population (59%) was beyond the sensitivity limit (>2.5 nm). These results indicate that a population (21%) of helices transitioned from a longer to a shorter inter-helix distance state when nucleotides were removed.

It is therefore suggested that a shift of the equilibrium between the positions of the α-1 and α-2 helices occurs upon nucleotide binding and release. In the ADP-bound state, the spectrum was an intermediate between those observed in the AMPPNP-bound state and no-nucleotide (NN) state. Fitting showed a fraction (25%) with a distance distribution centered at 1.40 nm and a full-width at half maximum of 0.24 nm, and the remaining spins (75%) were beyond the sensitivity limit (>2.5 nm).

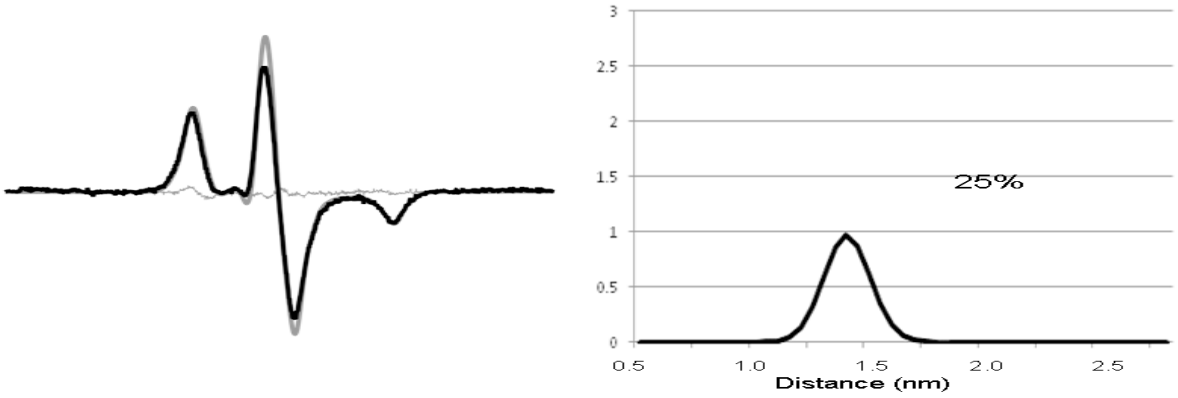

Figure III-6 Distance analysis of the EPR spectra from the double-labeled K68C/R114C kinesin mutant in the ADP-bound state with MTs. The spectra were obtained in the presence of ADP and MTs (See Material and Methods). All other conditions are as described in the legend of Figure III-4.

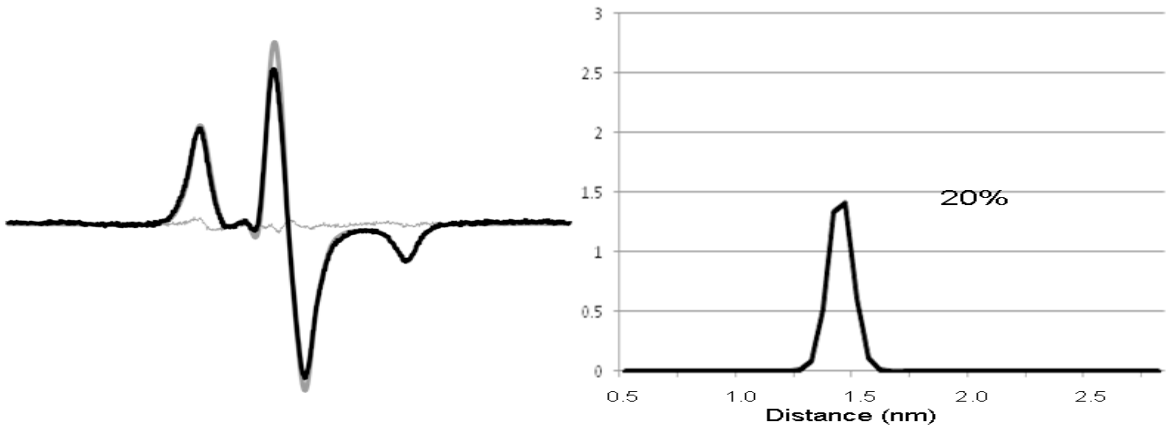

Figure III-7 Distance analysis of the EPR spectra from the double-labeled K68C/R114C kinesin mutant in the AMPPNP-bound state with MTs. The spectra were obtained in the presence of AMPPNP and MTs (See Material and Methods). All other conditions are as described in the legend of Figure III-4.

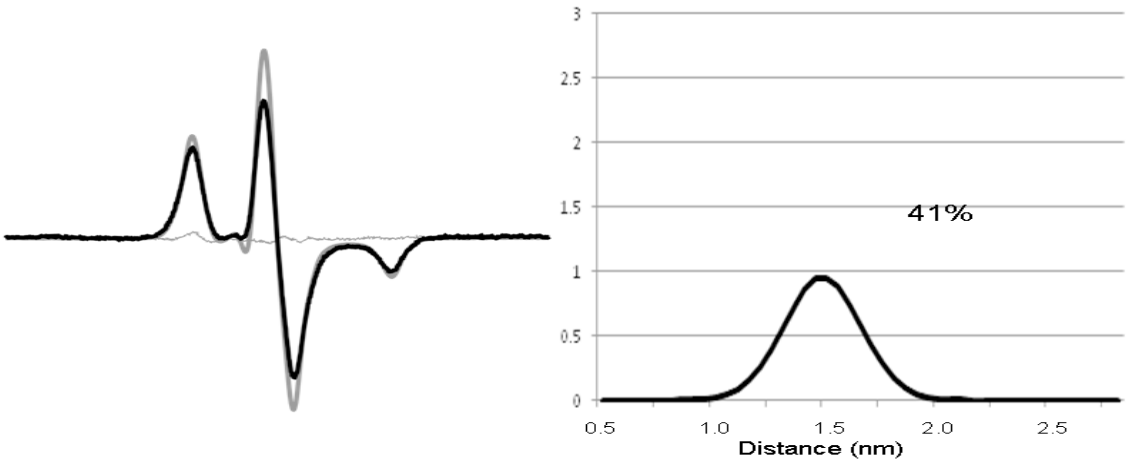

Figure III-8 Distance analysis of the EPR spectra from the double-labeled K68C/R114C kinesin mutant in the apo state with MTs. The spectra were obtained in the presence of apyrase and MTs (See Material and Methods). All other conditions are as described in the legend of Figure III-4.

Table III-3 Summary of distance distribution.

	Distance(nm)	full-width at half maximum(nm)	the noninteracting spins(%)
ADP	1.40	0.07	79
ADP+MT	1.40	0.24	75
AMPPNP+MT	1.43	0.13	80
NN(+apyrase)+MT	1.48	0.41	59

III.4 Implications of the conformational dynamics of the α-1 helix in the presence of MTs during the ATPase cycle

I have measured the mobility and distance of spin labels attached at to the α-1 and α-2 helices of kinesin. Inter-helix distance measurements in double-labeled, ADP-bound kinesin indicated that upon MT binding, the fraction of spins exhibiting a short inter-helix distance with a narrow distribution increased from 21 to 25%. On the other hand, the results from the single-labeled kinesins revealed that binding MTs increased the fraction of labels in the slow motional state by ~20% (thereby decreasing the fraction in the fast motional state by ~20%). The fraction of mobility change was much larger than that of distance change. Therefore, the effect of MT binding on mobility could be interpreted as inducing both (i) a transition to a state having a shorter inter-helix distance with a narrow distribution and (ii) a fast-to-slow shift in the equilibrium between side chain motional states in the conformations with longer inter-helix distances (Figures III-9).

Binding of nucleotide (ADP or AMPPNP) to kinesin in the presence of MTs increased the fraction of the fast mobility component by ~5% at the residues M68C and R114C. Inter-helix distance measurements also showed

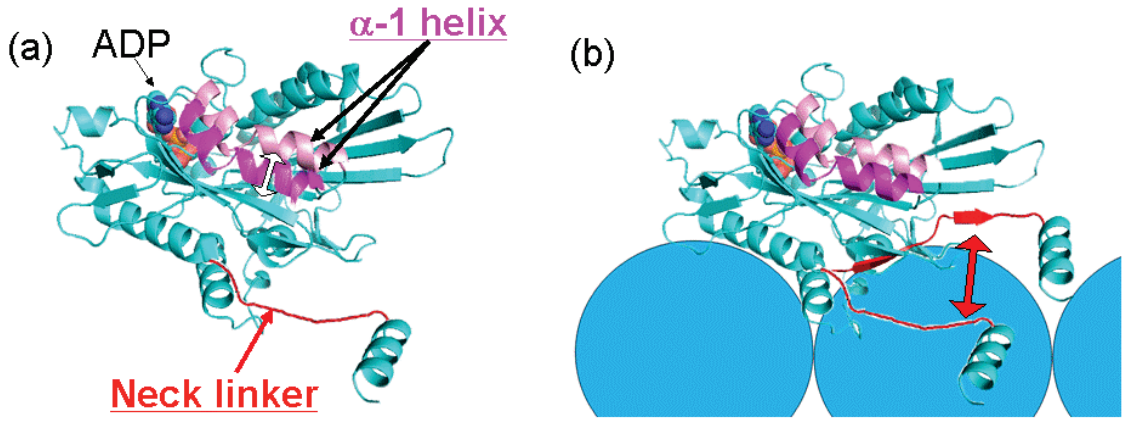

Figure III-9 Proposed conformations of the α-1 helix in the ADP states of kinesin in the absence (a) or presence (b) of MT. Blue semicircles show MT. ADP are shown as space-filling models. Color density of the α-1 helix (purple) shows the relative populations at longer and shorter distance from α-2 helix. (a) In MT-free state, the conformations with longer inter-helix distances are flexible (white arrow). (b) Note that the binding of MT to the motor domain, causing reduced flexibility of the backbone of the α-1 helix and partial binding of neck-linkers (red arrow).

that a substantial fraction (15-20%) of the helices transition from shorter to longer inter-helix distances upon nucleotide binding. Closer examination of the effects of nucleotide binding on residue mobility and inter-helix distance (i.e., AMPPNP and ADP effects on R114C and AMPPNP effects on M68C) revealed that they are quantitatively consistent when the equilibrium constants between fast and slow components are assumed to be 0.25 and 0 for the long and short distance states, respectively. However, the effect of ADP on the fraction of the fast mobility component at residue M68C appeared unexpectedly larger compared with the other residues, in which the effects of nucleotides were small or absent. It is further assumed that the equilibrium constant between the fast and slow components in the long distance state increased from 0.25 to 0.32 upon ADP binding at residue M68C, while it decreased from 0.25 to ~0.2 upon the binding of either AMPPNP or ADP at residues V62C, S66C, A67C, and I70C and from 0.6 to ~0.5 at residue K72C. Such small changes in the equilibrium constant might be produced by small changes in steric hindrance around the side-chains associated with nucleotide-induced changes in orientation, rotation, or bending of the α-1 helix in the long distance state. Figures III-10 shows the

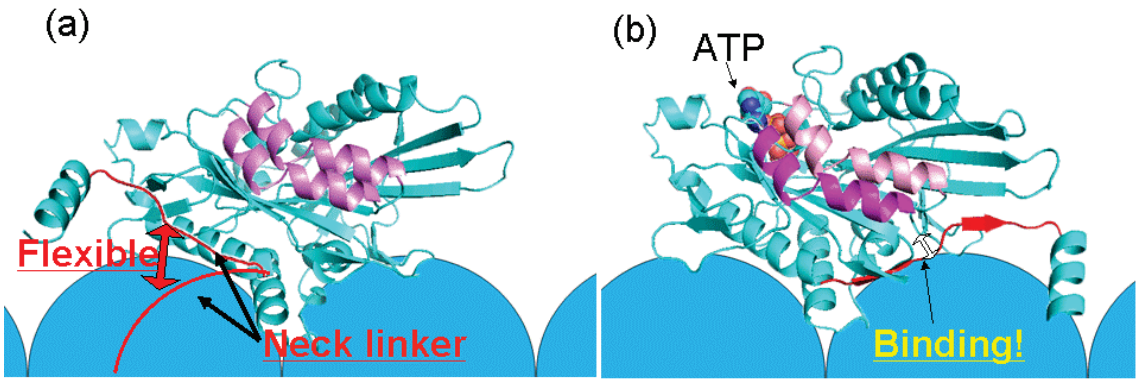

Figure III-10 Proposed conformations of the α-1 helix in the apo (a) and ATP (b) states of kinesin in the presence of MT. Color density of the α-1 helix (purple) shows the relative populations at longer and shorter distance from α-2 helix. Motor domain (cyan) and neck-linker (red) interactions are shown as white arrows. Blue hemicircles show MT. ATP is shown as a space-filling model. **(a)** In the apo state the dissociation of adenine ring of ADP from the N-terminal end of the α-1 helix, causing a shift in the positional equilibrium of the α-1 helix such that it is closer to the α-2 helix. This shift buries the C-terminal region of the α-1 helix, resulting in unbinding of neck-linker from the C-terminal region. Therefore neck linker is flexible (red arrow). **(b)** The binding of the adenine ring of ATP to the N-terminal end of the α-1 helix, cause a shift in the positional equilibrium of the α-1 helix away from the α-2 helix. This shift exposes the C-terminal region of the α-1 helix, resulting in rebinding of neck-linker to the C-terminal region. White arrow shows interaction between neck-linker and α-1 helix. (PDB ID:2KIN)

model of α-1 helix conformational change.

In conclusion, upon nucleotide binding in the presence of MTs, the two helices move apart in a substantial fraction of kinesins as a result of a shift in the positional equilibrium. The schematic representations of MT-dependent and nucleotide-dependent conformational changes of the α-1 helix are illustrated in Figures III-11, III-12, III-13, III-14, and III-15. It is an attractive possibility that upon binding of the N-terminal region of the α-1 helix to the adenine ring of ATP, the C-terminal region of the α-1 helix approaches the neck-linker and enhances the docking probability of the neck-linker to the motor domain. It should be noted that the position of the α-1 helix in the ADP-bound state is an intermediate between those in the AMPPNP-bound state and the NN state, but it is much closer to the former than the latter.

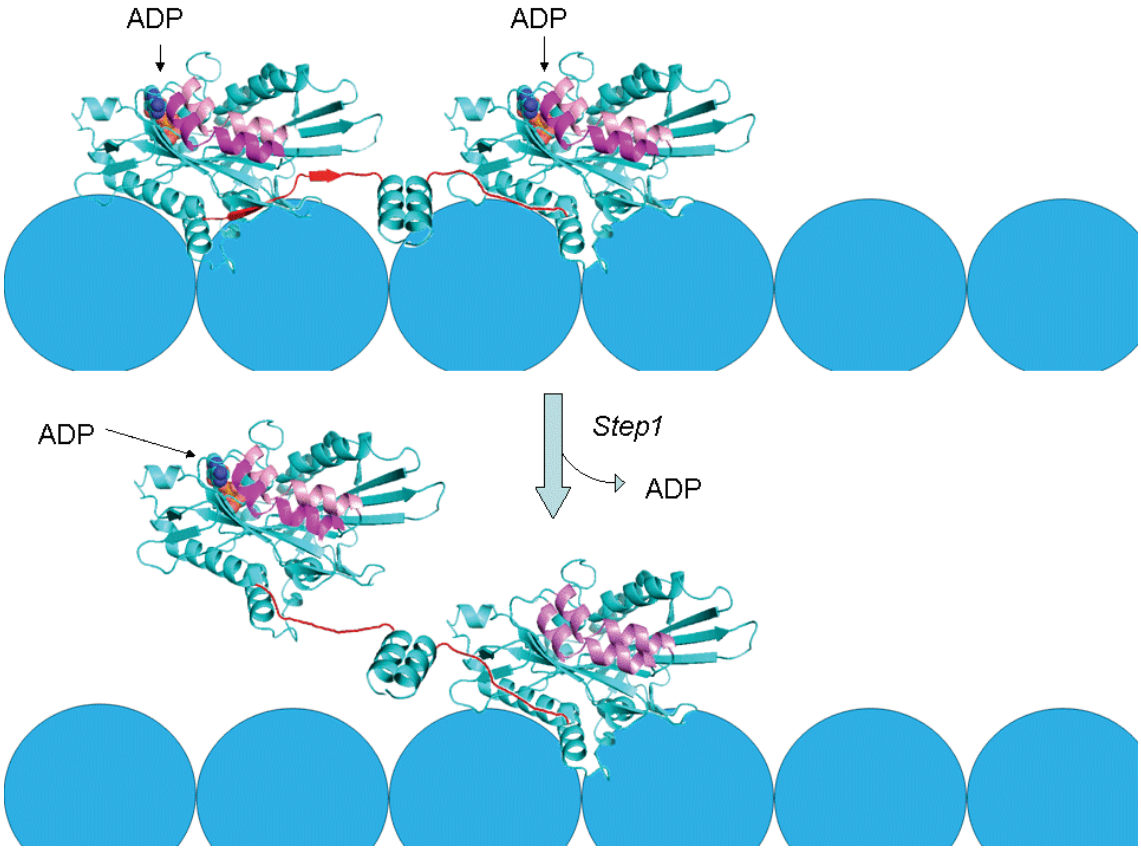

Figure III-11 Proposed conformations of the α-1 helix in the ATPase intermediate states of kinesin in the presence of MT (*Step1*). Motor domain and neck-linker interactions are shown as white arrows. The equilibrium shifts of α-1 helix position are represented in the purple arrows. The unbinding of a MT from the rear motor domain occurs. And the dissociation of adenine ring of ADP from the N-terminal end of the α-1 helix in the front motor domain, causing a shift in the positional equilibrium of the α-1 helix such that it is closer to the α-2 helix. This shift buries the C-terminal region of the α-1 helix, resulting in binding of ATP to the front head. (PDB ID:2KIN)

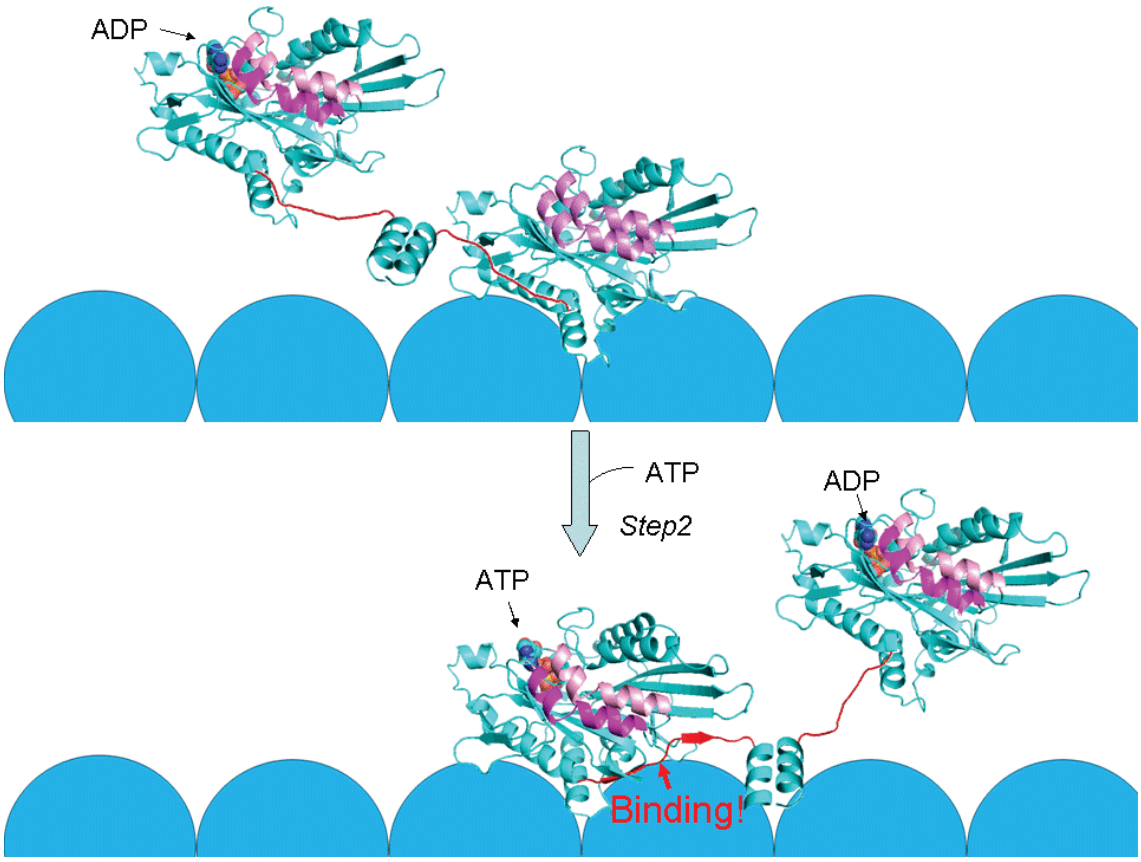

Figure III-12 Proposed conformations of the α-1 helix in the ATPase intermediate states of kinesin in the presence of MT (*Step2*). Motor domain and neck-linker interactions are shown as white arrows. The equilibrium shifts of α-1 helix position are represented in the purple arrows. The binding of the adenine ring of ATP to the α-1 helix N-terminal end of the front head causes a shift in the positional equilibrium of the α-1 helix away from the α-2 helix. This shift exposes the C-terminal region of the α-1 helix, resulting in binding of neck-linker to the C-terminal region of the head. (PDB ID:2KIN)

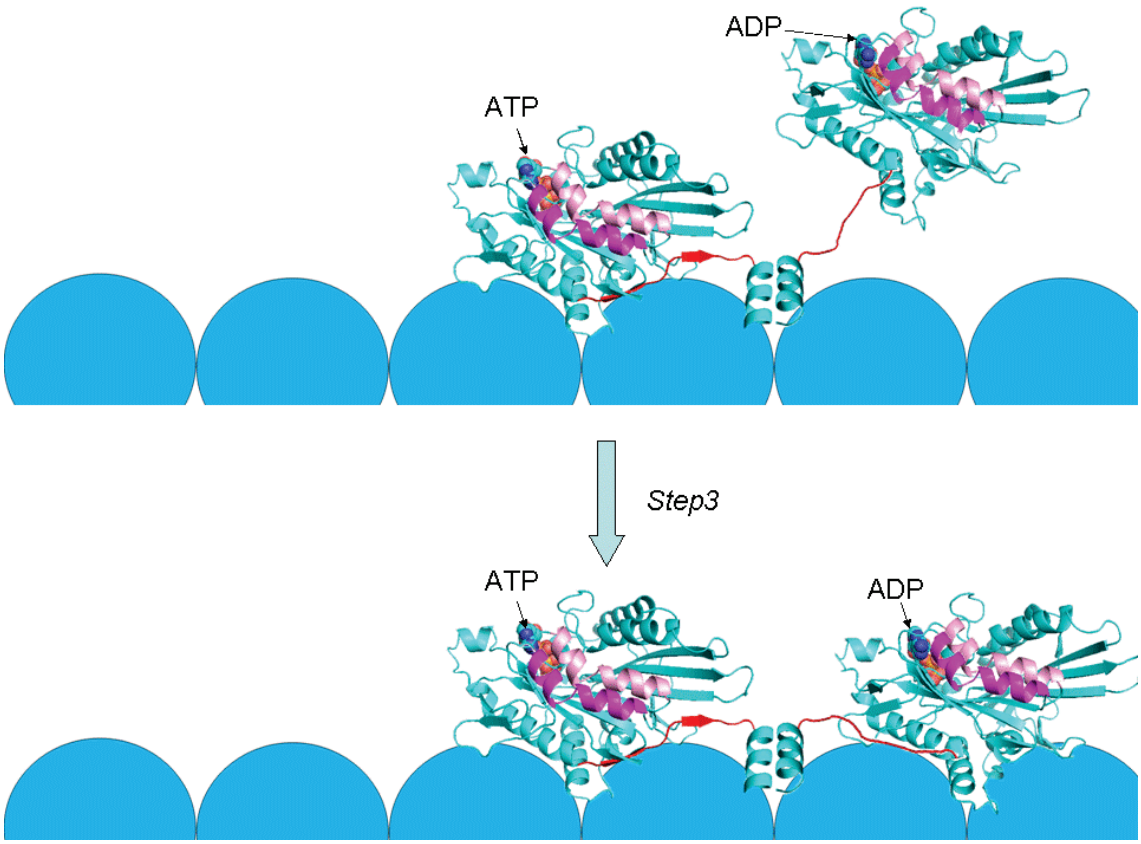

Figure III-13 Proposed conformations of the α-1 helix in the ATPase intermediate states of kinesin in the presence of MT (*Step3*). Motor domain and neck-linker interactions are shown as white arrows. The equilibrium shifts of α-1 helix position are represented in the purple arrows. The binding of the rear motor domain to MTs, causing reduced flexibility of the backbone of the α-1 helix and partial binding of neck-linker. The head became the new front head. (PDB ID:2KIN)

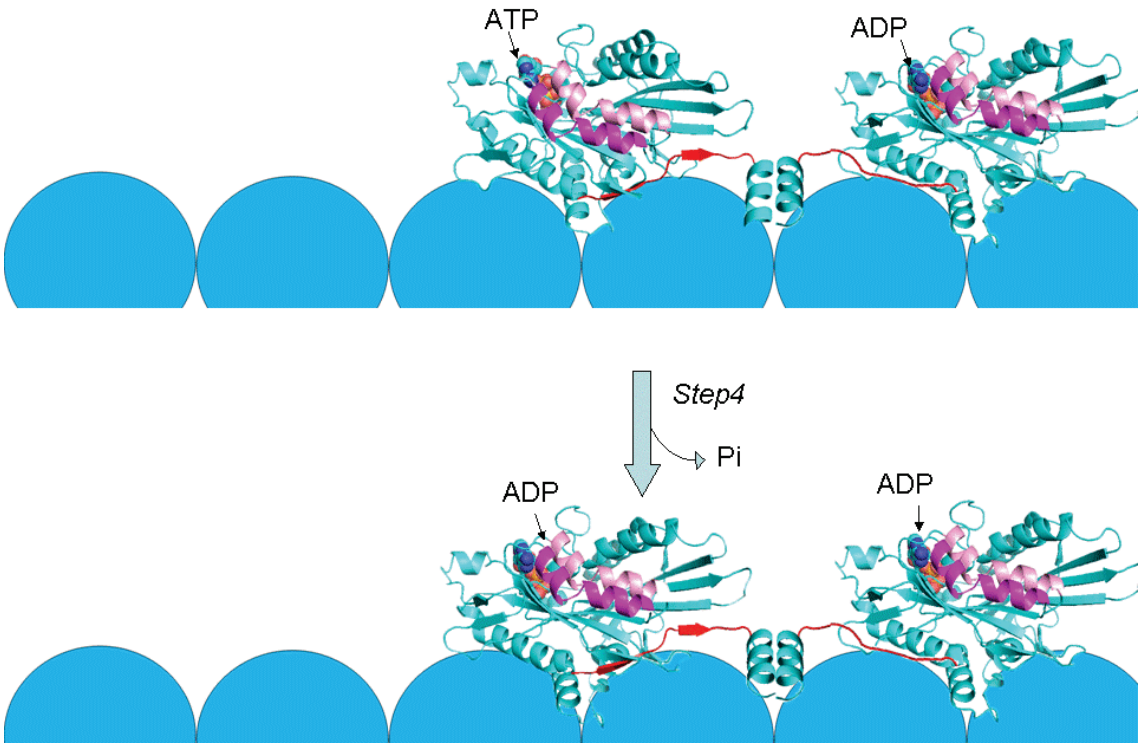

Figure III-14　Proposed conformations of the α-1 helix in the ATPase intermediate states of kinesin in the presence of MT (*Step4*). Motor domain and neck-linker interactions are shown as white arrows. The equilibrium shifts of α-1 helix position are represented in the purple arrows. The old front head hydrolyzes ATP. (PDB ID:2KIN)

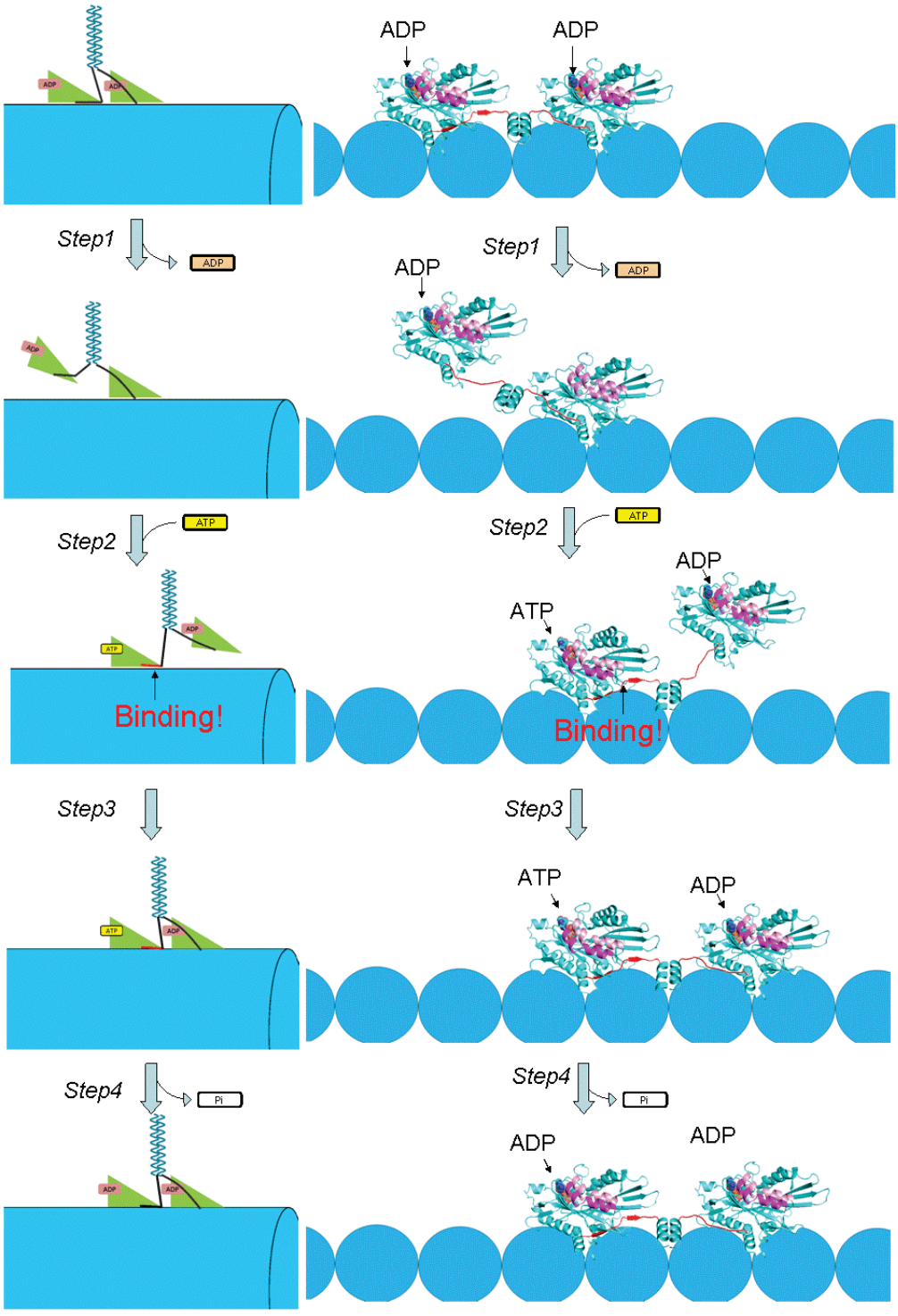

Figure III-15 Proposed conformations of the α-1 helix in the ATPase intermediate states of kinesin in the presence of MT. Summary of Figures III-11, III-12, III-13, and III-14. (PDB ID:2KIN)

III.5 Relation to other works

NL docking might be controlled by some other element, i.e., the structural linkage of switch II helix, switch I and P-loop to the γ-phosphate of ATP [Kikkawa et al., 2001; Hirose et al., 2006; Vale, 1996; Sindelar and Downing, 2007; Sindelar and Downing, 2010] as well as binding of the α-1 helix to the adenine ring (Figure III-16). The present study also predict that upon MT binding in the ADP state the α-1 helix is immobilized and undergoes a small shift of its positional equilibrium away from the adenine ring of ADP to lower the affinity and promote ADP release from a catalytic site. In the apo (NN) state, the α-1 helix moves further away and the catalytic site opens fully, while in the AMPPNP or ATP state the α-1 helix again approaches the adenine ring to close the catalytic site.

From chemical crosslinking experiments, Hahlen et al. [Hahlen et al., 2006] suggested that flexibility or structural changes in the α-1 helix is required for the ATPase activity of kinesin. High-resolution cryo-EM studies of human conventional kinesin bound to MT in the absence or presence of nucleotide were reported by Sindelar et al. [Sindelar and Downing, 2010]. This report showed that the electron density of the α-1 helix bound to

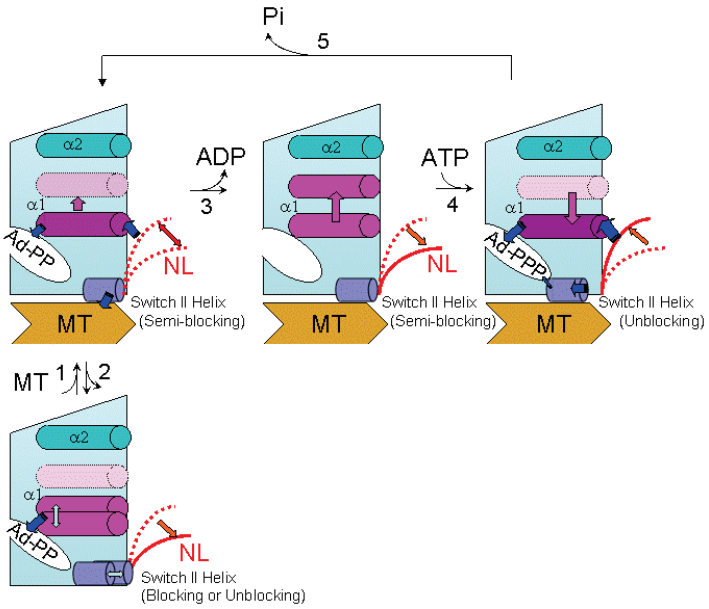

Figure III-16 Proposed conformations of the α-1 helix in the ATPase intermediate states of kinesin in the presence of MT. Protein-protein and protein-nucleotide interactions are shown as blue arrows. The equilibrium shift of the neck-linker binding and α-1 helix position are represented in the red and purple arrows, respectively. *Step 1*: The binding of a MT to the motor domain, causing reduced flexibility of the backbone of the α-1 helix and partial binding of NL. *Step 2*: The unbinding of a MT from the motor domain. *Step 3*: The dissociation of adenine ring of ADP from the N-terminal end of the α-1 helix, causing a shift in the positional equilibrium of the α-1 helix such that it is closer to the α-2 helix. This shift buries the C-terminal region of the AMPPNP in the α-1 helix, resulting in unbinding of neck-linker from the C-terminal region. *Step 4*: The binding of the adenine ring of ATP to the N-terminal end of the α-1 helix, causing a shift in the positional equilibrium of the α-1 helix away from the α-2 helix. This shift exposes the C-terminal region of the α-1 helix, resulting in rebinding of neck-linker to the C-terminal region. *Step 5*: ATP hydrolyzes.

presence of MTs was lower than that in the apo (NN) or ADP-bound state. This result suggests that the α-1 helix fluctuates in the AMPPNP state. This suggestion is consistent with our model, where the conformational state with a longer inter-helix distance exhibits high spin label mobility and high flexibility of the peptide side-chain and backbone. The fraction of kinesins with the longer inter-helix distance was larger in the AMPPNP-bound state than those in either the ADP-bound state or in the apo (NN) state in the presence of MTs. The spin label mobility in the AMPPNP state was also higher than that in the apo state, although it was almost indistinguishable (within error) from the ADP-bound state.

Cryo-EM study [Sindelar and Downing, 2010] also showed that the nucleotide binding pocket opens in the ADP state on MTs and fully in the apo state by displacement of the α-1 helix as well as switch I loop, as compared with that in the AMPPNP state on MTs. This view is consistent with our finding of the α-1 helix movement at the active catalytic site, displacing away from the adenine ring upon MT binding in the ADP state, further away in the apo state on MTs and approaching the ring in the AMPPNP state (See Figure III-10). More information from spin labels attached at the other

residues will be required to establish detailed structural changes within the kinesin motor domain at high resolution for comparison with the other structural studies.

III.6 Conclusions

For understanding of energy-transducing mechanisms, it is important to examine intra-molecular structures of transducer proteins during coordination between input and output. Kinesins are chemo-mechanical energy-transducing proteins. Neck-linker plays an important role as force generating element by docking and undocking on the motor core domain. Nucleotide-dependent changes in inter-molecular distance between two neck-linkers were previously found in our laboratory using spin labels attached to neck-linkers, suggesting a hand-over-hand mechanism.

However, it remains elusive how two motor domains coordinate at inter-molecular level by communication between catalytic site and neck-linker during hand-over-hand walking on microtubule. Here, I used site-directed spin labeling EPR to study kinesin monomer intra-molecularly and to directly detect the key structural change within the kinesin catalytic domain that defines the neck-linker power stroke as well as the nucleotide-induced displacement and dynamics of the α-1 helix. EPR measurements allowed direct and quantitative measurement of the mole

fraction of the helix structural states and thus of the equilibrium constants for the critical nucleotide-dependent helix movements. The results show that a shift in the equilibrium between two α-1 helix conformations occurs upon nucleotide binding and release at catalytic active site (adenine-ring binding site) and that this shift controls neck-linker docking onto the motor core. This provides direct insight into one of the most important aspects of kinesin enzymology, the coordination of ATP binding and the power stroke of the kinesin neck-linker. It will be interesting in the future to determine how forces across the motor domain-microtubule interaction acting between the motor domains in dimeric kinesin affect the coordination of the α-1 helix position, neck-linker docking, ADP release and ATP binding as well as how this coordination affects these forces.

IV References

Altenbach, C., Flitsch, S.L., Khorana, H.G., Hubbell, W.L. Structural studies on transmembrane proteins. 2. Spin labeling of bacteriorhodopsin mutants at unique cysteines, *Biochemistry* **28** (1989) 7806–7812.

Brady, S.T. A novel brain ATPase with properties expected for the fast axonal transport motor, *Nature* **317** (1985) 73-75.

Fajer, P., Song, L. Practical pulsed dipolar EPR (DEER), in: M. Hemminga, L. Berliner (Eds), *Biological Magnetic Resonance, Vol. 27, Springer New York* (2007) 95-128.

Goldman, S.A., Bruno, G.V., Freed. J.H. Estimating slow motional rotational correlation times for nitroxides by electron spin resonance, *J. Phys. Chem.* **76** (1972) 1858-1860.

Hackney, D.D. Kinesin ATPase: Rate-limiting ADP release, *Proc.Natl. Acad. Sci. U.S.A.* **85** (1988) 6314-6318.

Hahlen, K., Ebbing, B., Reinders, J., Mergler, J., Sickmann, A., Woehlke, G. Feedback of the kinesin-1 neck-linker position on the catalytic site, *J. Biol. Chem.* **281** (2006) 18868-18877.

Hilger, D., Jung, H., Padan, E., Wegener, C., Vogel, K.P., Steinhoff, H.J., Jeschke, G. Assessing oligomerization of membrane proteins by four-pulse DEER:

pH-dependent dimerization of NhaA Na+/H+ antiporter of *E. coli*, *Biophys. J.* **89** (2005) 1328–1338.

Hirokawa, N., Noda, Y., Okada, Y. Kinesin and dynein superfamily proteins in organelle transport and cell division, *Curr. Opin. Cell Biol.* **10** (1998) 60-73.

Hirose, K., Akimaru, E., Akiba, T., Endow, S.A., Amos, L.A. Large conformational changes in a kinesin motor catalyzed by interaction with microtubules, *Mol. Cell* **23** (2006) 913-923.

Hubbell, W.L., Cafiso, D.S., Altenbach, C. Identifying conformational change with site-directed spin labeling, *Nat. Struct. Biol.* **7** (2000) 735-739.

Hubbell, W.L., Gross, A., Langen, R., Lietzow, M.A. Recent advances in site-directed spin labeling of protein, *Curr. Opin. Struct. Biol.* **8** (1998) 649-656.

Jeschke, G. DeerAnalysis 2006 User's Manual, (2006)

Kikkawa, M., Sablin, E.P., Okada, Y., Yajima, H., Fletterick, R.J., Hirokawa, N. Switch-based mechanism of kinesin motors, *Nature* **411** (2001) 439-445.

Kull, F.J., Sablin, E.P., Lau, R., Fletterick, R.J., Vale, R.D. Crystal structure of the kinesin motor domain reveals a structural similarity to myosin, *Nature* **380** (1996) 550-555.

Mchaourab, H.S., Lietzow, M.A., Hideg, K., Hubbell, W.L. Motion of spin-labeled side chains in T4 lysozyme. Correlation with protein structure and dynamics, *Biochemistry* **35** (1996) 7692-7704.

Naber, N., Rice, S., Matuska, M., Vale, R.D., Cooke, R., Pate, E. EPR spectroscopy shows a microtubule-dependent conformational change in the kinesin switch 1 domain, *Biophy. J.* **84** (2003) 3190–3196.

Nakamura, M., Ueki, S., Hara, H., Arata, T. Calcium structural transition of human cardiac troponin C in reconstituted muscle fibres as studied by site-directed spin labelling, *J. Mol. Biol.* **348** (2005) 127-137.

Nitta, R., Kikkawa, M., Okada, Y., Hirokawa, N. KIF1A alternately uses two loops to bind microtubules, *Science* **205** (2004) 678-683.

Nitta, R., Okada, Y., Hirokawa, N. Structural model for strain-dependent microtubule activation of Mg-ADP release from kinesin, *Nat. Struct. Mol. Biol.* **15** (2008) 1067-1075.

Pannier, M., Veit, S., Godt, A., Jeschke, G., Spiess, H.W. Dead-time free measurement of dipole-dipole interactions between electron spins, *J. Magn. Reson.* **142** (2000) 331-340.

Rabenstein, M.D., Shin, Y.K. Determination of the distance between two spin labels attached to a micromolecule, *Proc. Natl. Acad. Sci. U.S.A.* **92** (1995) 8239-8243.

Rice, S., Cui, Y., Sindelar, C., Naber, N., Matuska, M., Vale, R.D., Cooke, R. Thermodynamic properties of the kinesin neck-region docking to the catalyic core, *Biophys. J.* **84** (2003) 1844-1854

Rice, S., Lin, A.W., Safer, D., Hart, C.L., Naber, N., Carragher, B.O., Cain, S.M., Pechatnikova, E., Wilson-Kubalek, E.M., Whittaker, M., Pate, E., Cooke, R., Taylor, E.W., Milligan, R.A., Vale, R.D. A structural change in the kinesin motor protein that drives motility, *Nature* **402** (1999) 778-784

Sack, S., Müller, J., Marx, A., Thormählen, M., Mandelkow, E.M., Brady, S.T., Mandelkow, E. X-ray structure of motor and neck domains from rat brain kinesin, *Biochemistry* **36** (1997) 16155-16165.

Sindelar, C.V., Budny, M.J., Rice, S., Naber, N., Fletterick, R., Cooke, R. Two conformations in the human kinesin power stroke defined by X-ray crystallography and EPR spectroscopy, *Nat. Struct. Biol.* **9** (2002) 844-848.

Sindelar , C.V., Downing, K.H. An atomic-level mechanism for activation of the kinesin molecular motors, *Proc. Natl. Acad. Sci. U.S.A.* **107** (2010) 4111-4116.

Sindelar, C.V., Downing, K.H. The beginning of kinesin's force-generating cycle visualized at 9Å resolution, *J. Cell Biol.* **177** (2007) 377-385.

Sugata, K., Nakamura, M., Ueki, S., Fajer, P.G., Arata, T. ESR reveals the mobility of the neck linker in dimeric kinesin, *Biochem. Biophys. Res. Commun.* **314** (2004) 447-451

Sugata, K., Song, L., Nakamura, M., Ueki, S., Fajer, P.G., Arata, T. Nucleotide-induced flexibility change in neck linkers of dimeric kinesin as detected by distance Measurements using spin-labeling EPR, *J. Mol. Biol.* **386** (2009) 626-636.

Tomishige, M., Vale, R.D. Controlling kinesin by reversible disulfide cross-linking: Identifying the motility-producing conformational change, *J. Cell Biol.* **151** (2000) 1081-1092.

Ueda, K. Distance Analysis between Actin and Tropomyosin in Ca2+ Regulated Skeletal Muscle Thin Filament using Isotopically Different Spin Labels, *Doctoral thesis* (2012)

Ueki, S., Nakamura, M., Komori, T., Arata, T. Site-directed spin labeling electron paramagnetic resonance study of the calcium-induced structural transition in the N-domain of human cardiac troponin C complexed with troponin I, *Biochemistry* **44** (2005) 411-416.

Vale, R.D. Switches, latches, and amplifiers: common themes of G proteins and molecular motors, *J. Cell Biol.* **135** (1996) 291-302.

Vale, R.D., Schnapp, B.J., Reese, T.S., Sheetz, M.P. Movement of organelles along filaments dissociated from the axoplasm of the squid giant axon, *Cell* **40** (1985) 449-454.

Verhey, K.J., Hammond, J.W. Traffic control: regulation of kinesin motors, *Nat. Rev. Mol. Cell Biol.* **10** (2009) 765-77.

Yamada, M.D., Maruta, S., Yasuda, S., Kondo, K., Maeda, H., Arata, T. Conformational dynamics of loops L11 and L12 of kinesin as revealed by spin-labeling EPR, *Biochem. Biophys. Res. Commun.* **364** (2007) 620-626.

Yamada, M.D., Nakajima, Y., Maeda, H., Maruta, S. Photocontrol of kinesin ATPase activity using an azobenzene derivative, *J. Biochem.* **142** (2007) 691-698.

Yildiz, A., Tomishige, M., Vale, R.D., Selvin, P.R. Kinesin walks hand-over-hand, *Science* **303** (2004) 676-678.

Acknowledgment

I would like to special thank my direct supervisor, Associate professor Toshiaki Arata.

I would also like to thank past Arata lab members, Dr. Akio Inoue, Dr. Shoji Ueki and Mr. Takanori Yanagi for their helping to ESR measurement and worthwhile advice.

Spatial thanks to Dr. Masafumi D. Yamada and Professor Shinsaku Maruta for advice about sample preparations. Without their contribution and support this study would not have been completed.

I spatial thank Dr. Fumio Tokunaga for helpful discussion. Without his advice my graduate study might not bear fruit.

I also wish to thank my committee members. They gave me some useful advices.

Publications

[1] Yasuda S., Yanagi T., Yamada M.D., Ueki S., Maruta S., Inoue A., Arata T. Nucleotide-dependent displacement and dynamics of α-1 helix in kinesin as revealed by site directed spin labeling EPR. *Biochem. Biophys. Res. Commun.* **443** (2014) 911-916.

[2] Yasuda S., Hara H., Tokunaga F., Arata T. Spatial arrangement of rhodopsin in retinal rod outer segment membranes studied by spin-labeling and pulsed electron double resonance., *Biochem. Biophys. Res. Commun.* **425** (2012) 134-137.

[3] Yamada M.D., Maruta S., Yasuda S., Kondo K., Maeda H., Arata T. Conformational dynamics of loops L11 and L12 of kinesin as revealed by spin-labeling EPR. *Biochem. Biophys. Res. Commun.* **364** (2007) 620-626.

[4] Arata T., Nakamura M., Ueki S., Sugata K., Aihara T., Ueda K., Yasuda S., Narumi R., Kusuhara H., Yamamoto Y. Dynamic structures of motor proteins myosin and kinesin, and switch protein troponin as detected by SDSL-ESR. *J. Electron. Microsc. (Tokyo)* **54** (2005) Suppl 1: i47-i51.